

International Journal of Innovations in Engineering Research and Technology

Volume No. 12

Issue No. 3

September - December 2025



ENRICHED PUBLICATIONS PVT.LTD

**JE - 18, Gupta Colony, Khirki Extn,
Malviya Nagar, New Delhi - 110017.**

E- Mail: info@enrichedpublication.com

Phone :- +91-8877340707

International Journal of Innovations in Engineering Research and Technology

Aims and Scope

"International Journal of Innovations in Engineering Research and Technology (IJIERT)" is an international journal. IJIERT is one of the fastest growing open access journals. It is an international online journal for the paper publication. The international journal provides the prospect to publish the original research papers with the author-friendly environment through its processes. This international journal is specially designed for paper publication in engineering, research, and technological advances.

IJIERT international journal supports the open access journals society by providing the free access to the published scholarly articles without any login or passwords. We being online journal taking care of the online presence and indexing of the articles published in various databases.

The paper submission in IJIERT is totally free of cost; however, after acceptance, we request the authors to pay the processing charges. We are working on high standards of scholarly journal publishing. Authors in search of international journals for paper publication will get fulfillment of publishing with our online international journal.

The scholarly journal is available online since 2014. The open access journal is highly indexed in databases. IJIERT is peer-reviewed, open access online journal aiming to serve the technical society with its high-quality technical contents. We are one of the best international journals for paper publication.

Members

ISSN: 2394-3696




Sr.No.	Name	Designation	Affiliation Details	Photo
1	Prof. Manoj R. Tarambale	Editor In-charge	Hod, Electrical, Marathwada Mitra Mandal's College of Engineering, Pune, Maharashtra, India	
2	Prof. Pravin R. Choube	Managing Editor	Assistant Professor, Marathwada Mitra Mandal's College of Engineering, Pune, Maharashtra, India	
3	Prof. Sudeep N, Upadhye	Managing Editor	VVP Institute of Engineering and Technology, Solapur, Maharashtra Email: upadhyesudeep@rediffmail.com	
4	Dr. MUTHE B.N. (SHEKHAR)	Associate Editor	Entrepreneur, Consultant and corporate trainer, Leanomics Consultancies Private Limited, Pune, Maharashtra, India Contact Email: shekharmuthe@gmail.com	
5	Dr. V. N. Gohokar	Advisor	Professor, All India Shri Shivaji Memorial Society's College of Engineering, Pune-411 001 Maharashtra, INDIA	
6	Dr. Tanaji Dabhade	Member	INTECSEA Attends Lamar University , Houston, Texas	
7	Dr. H.M.Dharmadhikari	Member	Professor, MIT, Aurangabad, Maharashtra, India	
8	Dr.L.M.KARTHIKEYAN	Member	Professor, Techno Global University, India	
9	Dr. Vishram N. Bapat	Advisor	ADJUNCT FACULTY, HVMP CET, Amravati	
10	Prof. G.K.Deshmukh	Associate Editor	Chairman, V.V.P. Institute of Engineering and Technology, Solapur, India	
11	Dr. P.D. Nemade	Associate Editor	Principal, SBPCOE, Indapur, India	
12	Mr. D.B. Mantri	Associate Editor	H.O.D. E&TC, VVPIET, Solapur, India	

Members

ISSN: 2394-3696

Sr. No.	Name	Designation	Affiliation Details	Photo
13	Moise, Daniel	Member	The Bucharest Academy of Economic Studies, Marketing Faculty, 41 Dacia Blvd., District 1, code 010511 Bucharest , ROMANIA	
14	Dr. S.A.Patil	Member, Editorial Board	Principal, AGPIT, Solapur	
15	Prof. V.V. Potdar	Member, Editorial Board	Vice Principal, AGPIT, Solapur	
16	Dr. S. R. Dulange	Member, Editorial Board	Dean Academics, AGPIT, Solapur	
17	Mr. S.H. Gidde	Member	Assistant Professor, SKNSCOE Korti, Pandharpur	
18	Dr. S.R. BOSELIN PRABHU	Advisor	VSB College of Engineering Technical Campus, Coimbatore, India Email: eben4uever@gmail.com	
19	Dr. Abhijeet J. Kaiwade	Member Editorial Board	Dr Professor, DY Patil Institute of MCA & MBA, Akurdi, Pune, India	
20	Dr. Iranna M. Korachagaon	Editor In Chief	Professor and HoD Electrical and Electronics Engineering, Vice Principal, Tontadarya College of Engineering, Gadag, Karnataka India	



Reviewers

Sr. No.	Name	Designation	Affiliation Details	Photo
1	Mr. Anand Magar	Reviewer, Computer Science & Engineering	Director, Savari Technologies, Pvt. Ltd. Pune, India	
2	Mrs. K.H. Wanjale	Reviewer, Computer Science and Engineering	Associate Professor, Vishwakarma Institute of Information Technology, Pune 411048	
3	Dr. L.Y. Waghmode	Reviewer, Mechanical Engineering	Vice Principal, Professor, ADCET, Ashta, Maharashtra, India	

Sr. No.	Name	Designation	Affiliation Details	Photo
4	Dr. N.D. Sangale	Reviewer, Engineering Mathematics	Professor, ADCET, Ashta, Maharashtra, India	
5	Mr. M.A. Tagare	Reviewer, Electrical Engineering	Associate Professor, Head of Department, FAMT, Ratnagiri	
6	Mr. S.A. Wamane	Reviewer, Electrical Engineering	Assistant Professor FAMT, Ratnagiri	
7	Dr. S.A. Patil	Reviewer, Mechanical Engineering	Professor, ADCET, Ashta, Maharashtra, India	
8	Mr. S.N. Satpute	Reviewer, Mechanical Engineering	Vice Principal, Head of Department, MMCOE, Karve Nagar, Pune, India	
9	Mr. S.A. Pattekari	Reviewer, Computer Science and Engineering	Dean, Rajarshi Shahu College of Engineering, Tathawade, Pune, India	
10	Mr. M.D. Patil	Reviewer, Electrical Engineering	Assistant Professor, ADCET, Ashta, Maharashtra, India	
11	Mr. Mocheb Lazam Shuwandy	Reviewer, Computer Science and Engineering	Associate Dean of the Faculty of Mathematics and Computer Science for Administrative Affairs,, Baghdad	
12	Dr. Shahera S. Patel	Reviewer, Electronics Engineering	Associate Professor, Sardar Patel University, V.V. Nagar, Gujrat, India	
13	Mr. S.A. Joshi	Reviewer, Environmental Engineering	Assistant Professor, KIT, Kolhapur, Maharashtra, India	
14	Mr. A.S. Vibhute	Reviewer, Electronics and Telecommunication Engineering	Associate Professor, HOD, BMIT, Solapur, India	
15	DR. MORE BABASAHEB MANIK	Reviewer, Engineering Physics	Associate Professor, BMIT, Solapur, India	

Sr. No.	Name	Designation	Affiliation Details	Photo
16	Mr. Ganesh Eknath Kondhalkar	Reviewer, Mechanical Engineering	H.O.D Anantrao Pawar College of Engineering & Research, Pune, India	
17	Mr. K.Gopala Reddy	Reviewer, Electrical and Electronics Engineering	Associate Professor, VVCE, Mysore, Karnataka, INDIA	
18	Mr. P.K.Magadum	Reviewer, Electrical Engineering	Assistant Professor, NBNSCOE, Solapur, India	
19	Mr. R.S. Khamitkar	Reviewer, Electronics and Telecommunication Engineering	Assistant Professor, NBNSCOE, Solapur, India	
20	Mr. S.R. Kshirsagar	Reviewer, Mechanical Engineering	H.O.D. SBPCOE, Indapur, India	
21	Mr. V. A. Chaudhari	Reviewer, Civil Engineering	Assistant Professor, SBPCOE, Indapur, India	
22	Mr. S.C.Mhamane	Reviewer, Electronics and Telecommunication Engineering	Research Scholar, VTU, Vishakhapattanam, India	
23	Mr. P.D.More	Reviewer, Electrical and Electronics Engineering	Assistant Professor, SGI, Atigre, India	
24	Mr. S.L.Pawar	Reviewer, Electronics and Telecommunication Engineering	H.O.D. , Fabtech COE, Sangola, India	
25	Mr. S.C. Jadhav	Reviewer, Electrical Engineering	Assistant Professor, MMCOE, Karve Nagar, Pune, India	
26	Mr. Bavdhane V. D.	Reviewer, Electrical Engineering	Assistant Professor, ZCOER, Pune	
27	Mr. Mane S. G.	Reviewer, Electrical Engineering	Assistant Professor, ZCOER, Pune	
28	Dinesh Kumar. A	Reviewer, Engineering Mathematics	H.O.D. and Assistant Professor, Dhanalakshmi Srinivasan Engineering College, Perambalur.	

Sr. No.	Name	Designation	Affiliation Details	Photo
29	Prof. Nitin S. Deshpande	Reviewer, Civil Engineering	VACOE, Ahamadnagar	
30	Prof. Amol R. Patil	Reviewer, Mechanical Engineering	Hod, Mechanical, VACOE, Ahamadnagar	
31	Prof. Bharat N. Kharad	Reviewer, Mechanical Engineering	Assistant Professor, Mechanical Department, VACOE, Ahamadnagar	
32	Prof. Ravindra M. Ghodke	Reviewer, Mechanical Engineering	Assistant Professor, Mechanical Department, VACOE, Ahamadnagar	
33	Prof. Jaydeep B. Ashtekar	Reviewer, Mechanical Engineering	Assistant Professor, Mechanical Department, VACOE, Ahamadnagar	
34	Prof. Anand K. Joshi	Reviewer, Mechanical Engineering	Hod, Mechanical Sandwich, VACOE, Ahamadnagar	
35	Prof. Vinay D. Patil	Reviewer, Mechanical Engineering	Assistant Professor, Mechanical Sandwich Department, VACOE, Ahamadnagar	
36	Mr. Tushar B. Waghmare	Reviewer, Electrical Engineering	Assistant Professor, Electrical Department, MMCOE, Karvenagar, Pune	
37	Prof. V.S. Dhongde	Reviewer, Electronics and Telecommunication Engineering	Assistant Professor, E&TC Department, VACOE, Ahamadnagar	
38	Prof. Puranik Vipin G	Reviewer, Electronics and Telecommunication Engineering	Assistant Professor, E&TC Department, VACOE, Ahamadnagar	
39	Prof. Joshi S.G	Reviewer, Information Technology Engineering	Hod, I.T., VACOE, Ahamadnagar	
40	Prof. Kshirsagar Mandar	Reviewer, Information Technology Engineering	Assistant Professor, I.T. Department, VACOE, Ahamadnagar	
41	Mr. S.R. Jagtap	Reviewer, Electronics and Telecommunication Engineering	Associate Professor and Head of The Department, RIT, Sakhrle	
42	Dr. S. A. Pardeshi	Reviewer, Electronics and Telecommunication Engineering	Professor, Department of E&TC, RIT, Sakhrle	
43	Dr. M. S. Patil	Reviewer, Electronics and Telecommunication Engineering	Professor and Head of Program (M.Tech. Electronics), RIT, Sakhrle	
44	Mr. M.S. Kumbhar	Reviewer, Mechanical Engineering	Associate Professor, E&TC Department, RIT, Sakhrle	
45	Mr. R.T. Patil	Reviewer, Electronics and Telecommunication Engineering	Associate Professor and Head of Program M.Tech. Electronics , RIT, Sakhrle	

Sr. No.	Name	Designation	Affiliation Details	Photo
46	Dr. A. B. Kakade	Reviewer, Electronics and Telecommunication Engineering	Associate Professor , E&TC Department, RIT, Sakhrale	
47	Mrs. S. S. Patil (Nalawade)	Reviewer, Electronics and Telecommunication Engineering	Assistant Professor , E&TC Department, RIT, Sakhrale	
48	Mr. A. R. Thorat	Reviewer,Electrical Engineering	Assistant Professor , Electrical Department, RIT, Sakhrale	
49	Mr. P. Sharath Kumar	Reviewer,Electrical Engineering	Assistant Professor , Electrical Department, RIT, Sakhrale	
50	Dr. Nagaraj V. Dharwadkar	Reviewer,Computer Science and Engineering	Associate Professor & Head of the CSE Department,RIT, Sakhrale	
51	Mr. Patil S. S.	Reviewer,Computer Science and Engineering	Assistant Professor, CSE Department, RIT, Sakhrale	
52	Mr. Patil S. S.	Reviewer,Computer Science and Engineering	Assistant Professor, CSE Department, RIT, Sakhrale	
53	Prof. Sudershan B.Gadwal	Reviewer,Mechanical Engineering	H.O.D (Mech.),AGPIT,Solapur	
54	Prof. Rahul V.Dandage	Reviewer, Mechanical Engineering	Asst. Professor, Mechanical Engg. Department, Rajendra Mane College of Engineering & Technology, Ambav, Maharashtra, India Email: dandagerahul@gmail.com	
55	Mr. T.D.Mali	Reviewer, Mechanical Engineering	Assistant Professor, Department of Production Engineering, SCOE,Vadgaon (BK), Pune-41 Email: tushar.aug1@gmail.com	

International Journal of Innovations in Engineering Research and Technology

(Volume No. 12, Issue No. 3, September - September 2025)

Contents

Sr. No.	Articles / Authors Name	Pg. No.
1	OPTIMAL PLACEMENT OF PHASOR MEASUREMENT UNIT (PMU) ON POWER NETWORK FOR REAL-TIME VOLTAGE MEASUREMENT <i>-Alex Aligbe, Monday F. Ohemu Adeleke A. Hafiz I Aiyudubie S. Uyi</i>	1- 11
2	MECHANICAL PROPERTIES OF DRAMIX HOOKED END STEEL FIBER REINFORCED CONCRETE <i>-Falmata A. Mustapha Department of Civil Engineering Technology,</i>	12 - 22
3	EVALUATING THE FLEXURAL STRENGTH OF CORRODED REINFORCED CONCRETE BEAMS <i>-Ibim Green, Kelechi Ugoji</i>	23 - 27
4	THE EFFECT OF HYBRID STEEL FIBER ON CONCRETE PERFORMANCE <i>-Ibim Green, Kelechi Ugoji</i>	28 - 34
5	DEVELOPMENT OF ROBOTIC SYSTEM FOR SEGREGATION OF METALLIC COMPONENTS <i>-Adyuth Hisham Babu Syed, Jonah N., Binil Mohan</i>	35 - 40

OPTIMAL PLACEMENT OF PHASOR MEASUREMENT UNIT (PMU) ON POWER NETWORK FOR REAL-TIME VOLTAGE MEASUREMENT

Alex Aligbe,

Department of Electrical and Electronics Engineering, Air Force Institute of Technology, Kaduna, Nigeria aligbealexprof@gmail.com

Monday F. Ohemu

Department of Electrical and Electronics Engineering, Air Force Institute of Technology, Kaduna, Nigeria monfavour@gmail.com

Adeleke A. Hafiz1

Department of Electrical and Electronics Engineering, Air Force Institute of Technology, Kaduna, Nigeria, h.adeleke@afit.edu.ng

Aiyudubie S. Uyi

Department of Telecommunication Engineering, Air Force Institute of Technology, Kaduna, Nigeria As.uyi@fit.edu.ng

ABSTRACT

Due to the advancement in electrical power systems, there is need for control, monitoring and protection so as to improve the efficiency, reliability and security of the power network. Phasor Measurement Units (PMU) as the ability to perform enlisted task also perform operations in real-time and dynamic monitoring scenario. The aim of this research work was to optimally site PMUs on IEEE 14- Bus and IEEE 33-Bus network using Graph Theoretic Procedure Method (GTPM) with the ability to maximally observe the whole power network. For IEEE 14-Bus network 5 PMUs were required while for IEEE 33-Bus network 14 PMUs were required for full observability of the networks. The GTPM was compared with previous method used on IEEE 14-Bus network. The PMUs measured voltage magnitude and phase angle was compared with load flow analysis using Newton Raphson method.

Keywords: Phasor Measurement Units, Graph Theoretic Procedure Method, Optimal Placement, Power Network, Voltage Magnitude.

Introduction

Supervisory control and data acquisition (SCADA) was the traditional method of collecting data from wide area network, but it have drawbacks such as slow static measurement due to its inability to observe the dynamic state of the system, unable to synchronize data and inability to make accurate state estimators of the network that can cause blackout[1].

Due to the advancement in power systems, there is need for fast, accurate and synchronization of measured data from distance location for monitoring to improve the efficiency, reliability and security of the power network[2]. Phasor Measurement Units (PMU) are mainly used to monitor power system for critical conditions such as, voltage variation, faulty conditions, or any contingencies in a power system, it can also act as a fault recorder in power systems by recording waveforms.

It can be deployed in real-time or dynamic monitoring scenario. The real-time monitoring scenario can be achieved by deploying Global Positioning system (GPS)[3]. PMU with sufficient numbers of channels can be installed on node bus to measure voltage magnitude and voltage phasor of the installed bus and the current phasor of all the branches connected to the node bus, these can help to improved protection, monitoring, and control of the system in a smart grid[3]. The cost price of PMU device ranges from \$40,000 to \$180,000 depending on the number channels the device is having[1]. Installing PMU at every bus on the network is not economical; there is need to optimally placed PMU on power networks to minimize cost. In 2014, about 1100 PMUs were installed on United State Eastern interconnection network, the PMUs were able to monitor the transmission system[4].

Placement of PMU in a modern power network is a big challenge because of the financial implication, there is need for researcher to find possible ways to minimize cost. We have two methodologies that have been used in literature to address the purpose of optimal PMU allocation problem: (i) allocation of PMU to monitor the dynamic response of the system and (ii) development of list of allocation based on observability of the network. The dynamic response method gives a coherent picture of the power network and are mainly used to analyze voltage stability to avoid voltage collapse[5], protection, and assessment of the voltage security[6][7] while allocation based on observability are deployed to ensure that the whole network is properly observed, placing PMU on every bus of the network is not economical, that is why there is need for optimal placement of PMU for as long all buses are observed, this method was demonstrated in [8][1][9][10].

To achieved optimal placement of PMU, three method have been applied which are: (i) mathematical approach by deploying the mathematical model of the system[11], an example of a mathematical method used by researcher are: integer linear programming; mixed integer linear programming; (ii) meta-heuristic algorithms: In [12], Genetic Algorithm (GA) was deployed for optimally placed PMU, considering the observability and security of the network; Tabu search algorithm was used to optimally placed PMU for effective observability of the full network [13]; Exponential Binary Particle Swarm Optimization (EBPSO) was developed to find multiple solution of PMU placement for a smart grid application [14]; Grey Wolf Optimization Algorithm (GWOA) was developed to monitor the power network whenever the power company loses full observability of the system and (iii) graph theory approach

Power System Observability and PMU Sitting Formulation.

A power network is said to be observable when all the state variable of the network are estimable. This is when the network voltage magnitude and voltage phasor of all the buses are measurable. When power system changes state, it affects the measured data and the network topology at any time, if this condition occurs, network observability becomes necessary. Network observability depends on the numerical and topological structure of the network. The topological approach is based on the information about measurement type, network connectivity and locations while the numerical approach is based on the gain matrix or the numerical factorization Jacobian matrix measurement information.

Topology Observability Approach

This method deals with the network structure, type of measurement and locations by identifying observable buses and the one around it. Topology observability methods have fast converged speed compare to numerical observability method and are highly implemented in software packages. So, in optimal PMU placement is to minimize the number of PMUs and their installation locations such that the

whole network becomes observable, topological observability method have proven to be more reliable and faster in observing network. From literature, it was observed that researchers develop different rules in analyzing network observability, the rules are as follows [15]:

- i. When a PMU is placed on a particular bus, the voltage and current phasor of that bus and its interconnected branches are known, it is called direct measurement;
- ii. Whenever the voltage phasor at both end of a branch is observed, the current phasor of the branch can be directly obtained, also, if the voltage phasor at one end of a branch is observed, the voltage and current phasor of the other end of the branch can be directly obtained, these type of measurement is called pseudo measurements;
- iii. For N-bus network with zero-injection bus can be express as;

$$\sum_{k=1}^N Y_{ik} \cdot V_k = 0 \quad (1)$$

Where; Y_{ik} represent the admittance matrix of the k- bus and V_k represent the k-bus voltage phasor of the network. Therefore, if a zero-injection bus exists without PMU, and the interconnected branches current phasor are all observed except one, then the current phasor of the unobserved branch could be calculated using Kirchhoff's current law (KCL);

- iv. If a zero-injection bus with unknown voltage phasor exist on the network and voltage phasor of its adjacent buses are all known, the voltage phasor of the zero-injection node can be obtained by deploying Nodal analysis; and
- v. If a group of adjacent zero-injection buses voltage phasors are unknown and the voltage phasors of all adjacent buses to the group are known, then the voltage phasor of the zero-injection buses can be obtained by deploying Nodal analysis.

The measurements obtained from rule (iii-v) are called extended measurements.

PMU Sitting Mathematical Formulation

The optimal placement problem (OPP) formulations in respect to topological observability approach is as follow[16];

$$f(w) = \min \sum_{i=1}^P w_i \quad (2)$$

Subject to $Af(x) \geq B$

Where;

$f(w)$ represent objective function for Optimal PMU Placement (OPP);

w_i refers to the PMU's installed on the network; and P is the total number of network buses.

$$B_i = \geq [1 \ 1 \ 1 \ 1 \ \dots \ \dots \ 1 \ 1 \ 1]^T \quad (3)$$

$[x_i]$ is the PMU positional matrix associated with node i as defined in eq.(4)

$$x_i = \begin{cases} 1, & \text{if PMU is installed on node } i \\ 0, & \text{if PMU is otherwise} \end{cases} \quad (4)$$

The objective function $f(x)$ is subjected to observability constraint to ensure all buses on the network are observed; it is given in eq. (5).

$$F_i = \sum_{j=1}^N A_{ij} x_j \geq Y \quad (5)$$

Where;

Y is the N size of vector whose element are all 1

F_i is the observability constraint of buses relating to the PMU bus;

$$F_i = \begin{cases} \neq 0 & \text{if node } i \text{ is observable} \\ = 0 & \text{if node } i \text{ is otherwise} \end{cases} \quad (6)$$

A_{ij} is the connectivity binary matrix of the network, whose elements are;

$$A_{ij} = \begin{cases} 1 & \text{if node } i = \text{node } j \\ 1 & \text{if node } i \text{ and } j \text{ are connected} \\ 0 & \text{if node } i \text{ and } j \text{ are otherwise} \end{cases} \quad (7)$$

The graphical representation of IEEE 14-bus and IEEE 33-bus network are shown in figure 1 and 2.

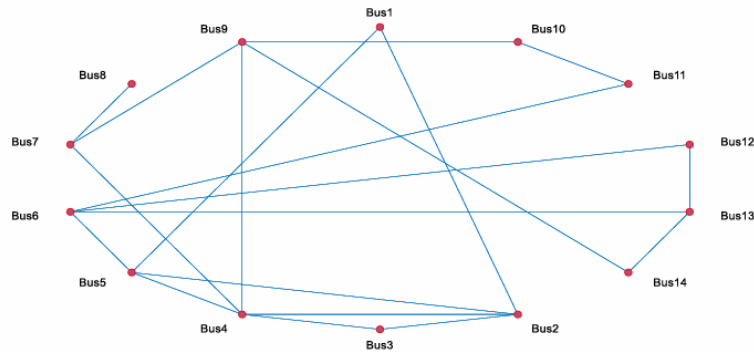


Figure 1: Graphical Representation of IEEE 14-bus Network

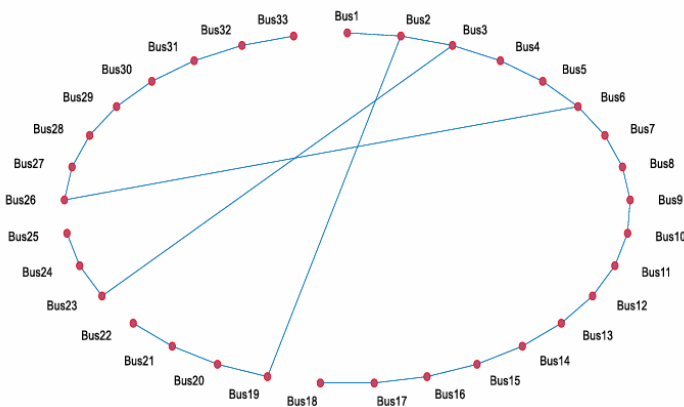


Figure 2: Graphical Representation of IEEE 33-bus Network

IEEE 14-bus network topology shown in figure 1 is represented in binary connectivity matrix shown in eq. (8) to solve Optimal PMU Placement (OPP) problem according to eq. (6).

$$A = \begin{bmatrix} 1 & 1 & 0 & 0 & 1 & 0 & 0 & 0 & 0 & 0 & 0 & 0 & 0 & 0 & 0 \\ 1 & 1 & 1 & 1 & 1 & 0 & 0 & 0 & 0 & 0 & 0 & 0 & 0 & 0 & 0 \\ 0 & 1 & 1 & 1 & 0 & 0 & 0 & 0 & 0 & 0 & 0 & 0 & 0 & 0 & 0 \\ 0 & 1 & 1 & 1 & 1 & 0 & 1 & 0 & 0 & 0 & 0 & 0 & 0 & 0 & 0 \\ 1 & 1 & 0 & 1 & 1 & 1 & 0 & 0 & 0 & 0 & 0 & 0 & 0 & 0 & 0 \\ 0 & 0 & 0 & 0 & 1 & 1 & 0 & 0 & 0 & 0 & 1 & 1 & 1 & 0 & 0 \\ 0 & 0 & 0 & 1 & 0 & 0 & 1 & 1 & 1 & 0 & 0 & 0 & 0 & 0 & 0 \\ 0 & 0 & 0 & 0 & 0 & 0 & 1 & 1 & 0 & 0 & 0 & 0 & 0 & 0 & 0 \\ 0 & 0 & 0 & 1 & 0 & 0 & 1 & 0 & 1 & 1 & 0 & 0 & 0 & 0 & 1 \\ 0 & 0 & 0 & 0 & 0 & 0 & 0 & 0 & 1 & 1 & 1 & 0 & 0 & 0 & 0 \\ 0 & 0 & 0 & 0 & 0 & 1 & 0 & 0 & 0 & 1 & 1 & 0 & 0 & 0 & 0 \\ 0 & 0 & 0 & 0 & 0 & 1 & 0 & 0 & 0 & 0 & 1 & 1 & 0 & 0 & 0 \\ 0 & 0 & 0 & 0 & 0 & 1 & 0 & 0 & 0 & 0 & 0 & 1 & 1 & 0 & 0 \\ 0 & 0 & 0 & 0 & 0 & 1 & 0 & 0 & 0 & 0 & 0 & 1 & 1 & 1 & 1 \\ 0 & 0 & 0 & 0 & 0 & 0 & 0 & 0 & 1 & 0 & 0 & 0 & 1 & 1 & 1 \end{bmatrix} \quad (8)$$

Identification of Minimum Number of PMUs Buses

A PMU located on a bus should be able to measure the bus voltage and the current phasor including the interconnected buses. The system observability is complete when all the synchronized measurements provided by the PMUs are obtained. Besides we ensure the minimum number of PMUs measurement needed for the network observability are available (i.e. all nodes are observed). Under these conditions, the bus candidates for locating the PMUs, that is, the PMU-buses are those represented with larger number of interconnected branches.

For PMU-buses to be identified on a power network, let consider a power network that consists of an N-buses and L- branches as shown in eq.(9).

$$Q = A^T A \quad (9)$$

Where; A is the $L \times N$ incidence matrix, N is an $n \times n$ dimensional matrix and Q is an $n \times n$ symmetrical matrix respectively.

The ith diagonal element of Q, namely Q_{ii} , describes the connectivity degree characterizing the ith bus.

The off-diagonal elements in the same row or column, $Q_{ij} (i \neq j)$, indicate if buses i and j are directly connected (namely $-Q_{ij} = -1$) or not (namely $-Q_{ij} = 0$). It should be noted that the non-zero off-diagonal elements can be nothing other than -1 .

By applying a permutation matrix P to Q we obtain:

$$Q^* = P Q P^T \quad (10)$$

The matrix Q^* has been arranged in a descending order of the connectivity degree. This matrix allows us to define a priority list of the PMU-buses candidates. Starting from this list, the PMU-buses will be selected by applying an iterative algorithm based on the topological network observability analysis.

Load Flow Formulation Analysis

The purpose of conducting load flow analysis on power network is to get complete information about the voltage profile on each bus and the power losses of the network [17]. Numerical method is used provide solution to load flow problems due to their nonlinear nature of the problem.

The equation for a balance power system, are written in two equations which are; real and reactive power for each bus.

For real power balance equation is

$$0 = -P_n + \sum |V_n| |V_m| (G_{nm} \cos \theta_{nm} + j B_{nm} \sin \theta_{nm}) \quad (11)$$

While the balance equation for the reactive power can be expressed as

$$0 = -Q_n + \sum |V_n| |V_m| (G_{nm} \sin \theta_{nm} + j B_{nm} \cos \theta_{nm}) \quad (12)$$

Where P_n and Q_n are the net injected real and reactive power at bus n , G_{nm} and B_{nm} represent real and imaginary part of the element in the n^{th} and m^{th} bus admittance matrix Y_{BUS} and θ_{nm} is the difference in voltage angle between n^{th} and m^{th} buses.

The complex power equation is written as [18];

$$S_n = P_n + jQ_n$$

$$\text{Where } S_n^* = V_n^* I$$

$$I = \sum_{m=0}^N Y_{nm} V_m$$

$$P_n - jQ_n = |Y_{nm} V_m V_n| \text{ang}(\theta_{nm} + \delta_m - \delta_n) \quad (13)$$

Separating the real and imaginary part from eq. (10), we can obtain;

$$P_n = \sum_{m=0}^N |Y_{nm} V_m V_n| \cos(\theta_{nm} + \delta_m - \delta_n) \quad (14)$$

$$Q_n = -\sum_{m=0}^N |Y_{nm} V_m V_n| \sin(\theta_{nm} + \delta_m - \delta_n) \quad (15)$$

Where δ_m and δ_n are the voltage phase angle of bus m and n respectively and N is the total number of buses [17].

Newton Raphson Method was used to analyze the load flow for IEEE 33-bus network using PSAT 2.1.11 Software, the voltage magnitude in (P.U) obtained from the analysis is shown in figure 2.

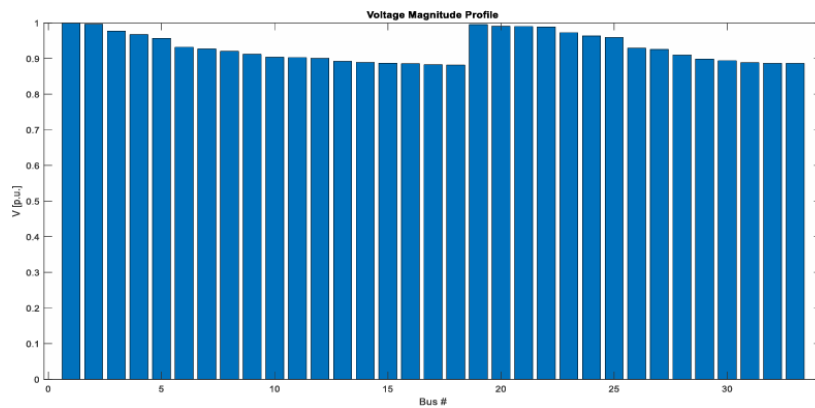


Figure 3: voltage magnitude for IEEE 33-bus network

State variable Estimation on Power System

The mathematical model use to estimate power system state variables is given as [19]:

$$z = y(x) + v \quad (16)$$

Where x represent the estimated state variables which are presented in matrix form as; $\begin{bmatrix} \delta^T \\ V^T \end{bmatrix}$ where δ = bus voltage angle and V = bus voltage magnitude, $z = (m \times 1)$ measurement vector, $v = (m \times 1)$ measurement error vector, and $y(.) = (m \times 1)$ vector of nonlinear functions [19].

The state variables estimated problem according to eq. (16) can solved using iterative method, which is given as:

$$[\Delta x^i] = G(x^i)^{-1} H^T(x) W [\Delta z^i]; i = 0, 1, 2, 3, \dots \dots \dots (17)$$

$$\text{Where } x^{(i+1)} = [\Delta x^i] + x^i; [\Delta z^i] = z - y(x^i)$$

$$\text{and } G(x^i) = H^T(x) W H(x^i)$$

where W is the diagonal matrix whose element are the measurement weighting factors, $H(x)$ is the jacobian matrix of $y(x)$, and $G(x)$ is the gain matrix.

The Research Methodology

This section discusses about the method deployed in optimal placement of PMUs in IEE 14-bus and IEEE 33bar network for complete observability and measurement of voltage magnitude and phase angle using Graph Theory Algorithm. The power network was model on PSAT 2.1.11 software.

Graph Theoretic Procedure

In a power system, a network can be represented by an undirected graph $G = (V, E)$ [20], where $V = (v_1, v_2, v_3, v_4, \dots, v_n)$ is called vertex, it is representing the buses on the network, and E is called edges and represent the transmission lines and transformers. A power network graphical $(e_1, e_2, e_3, e_4, \dots, e_n)$ representation consists of a set of vertex (buses) connected by set of edge (transmission lines) [21]. The graphical representation of IEEE 14-bus and IEEE 33-bus is shown in figure1 and 2. And the connectivity matrix of a IEEE14-bus is represented in eq (8).

Load Flow Analysis Using Newton Raphson Algorithm

Assume that all the buses on the network are PQ buses, the load flow solution must agree with non-linear algebraic equations in figure (18) and figure (19).

The research work flow chart model

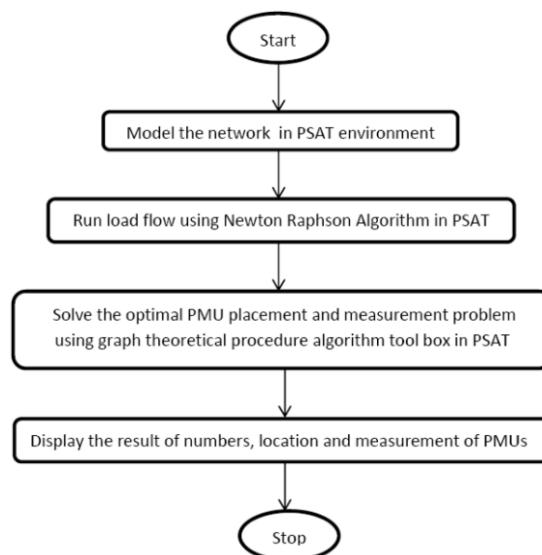


Figure 4: The research flow chart on PSAT software

Result and Discussion

Figure 5 shown below represent the load flow analysis and PMU measured voltage magnitude for IEEE 33- Bus network. The PMU was optimally placed on 14 buses and it was able to observe the voltages in all the buses. The accuracy of the PMU measurement ranges from 97- 99%. Figure 6; represent the load flow and PMU phase angle measurement.

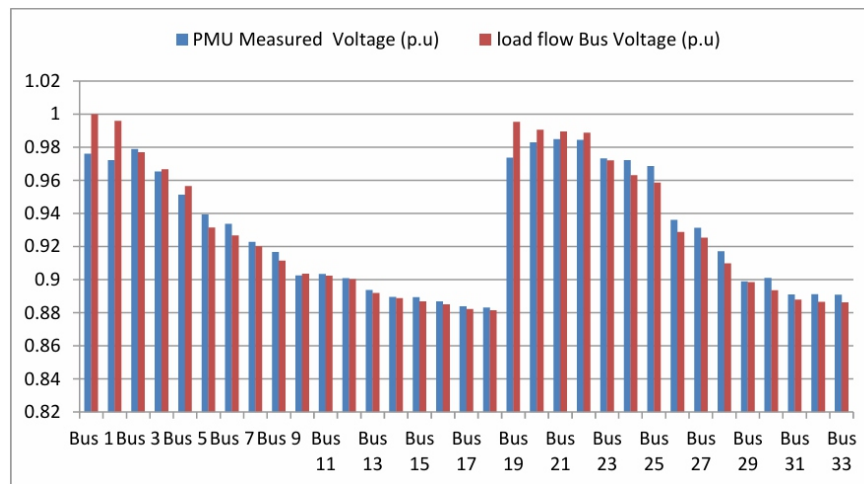


Figure 5: the load flow and the PMUs measured voltage values (p.u)

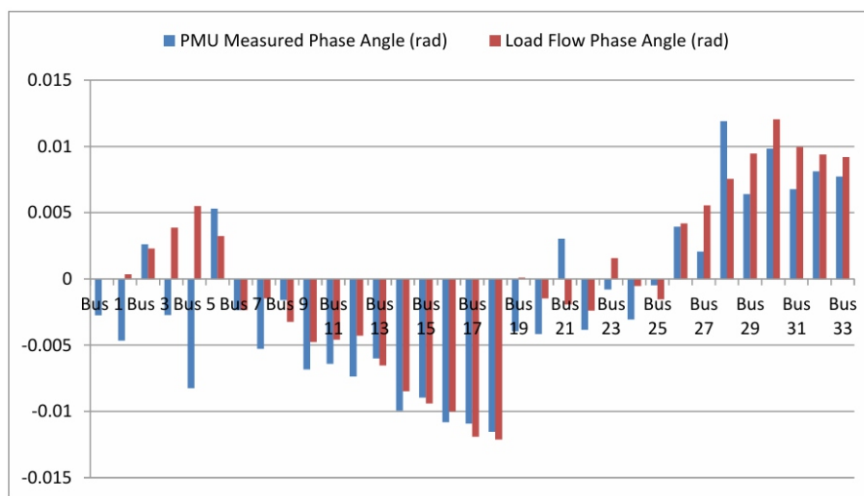


Figure 6: Phase angle values from load flow analysis and PMUs for IEEE 33 bus.

Figure 7a and 7b shows the plot of voltage magnitude and phase angle for IEEE 14 bus network as a result from load flow analysis and PMUs measured values. PMUs were optimally installed in five buses on the network and able to observed and measured voltages on all the buses on the network.

Graph theoretic procedure (proposed method) were compared with previous method on IEEE 14 – Bus network in table 1, it was observed that the proposed method was able to optimally placed PMUs on five (5) buses while other methods except Depth first method were able to optimally placed on four (4) buses. Table 2 shows the bus location for optimally siting PMUs on IEEE 33-Bus network using Graph theoretic procedure method.

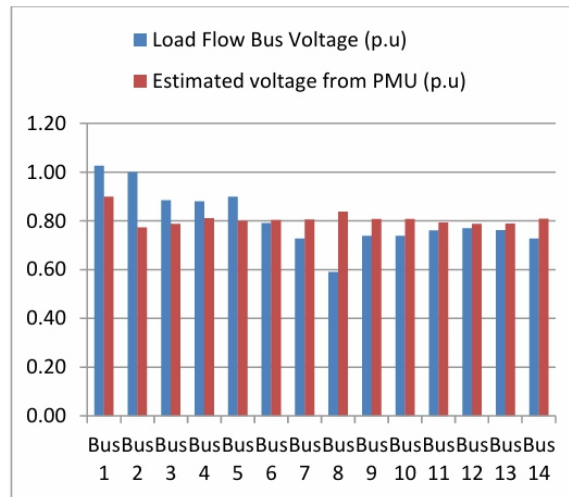


Figure 7a: load flow and PMU measured voltage values for IEEE 14 bus

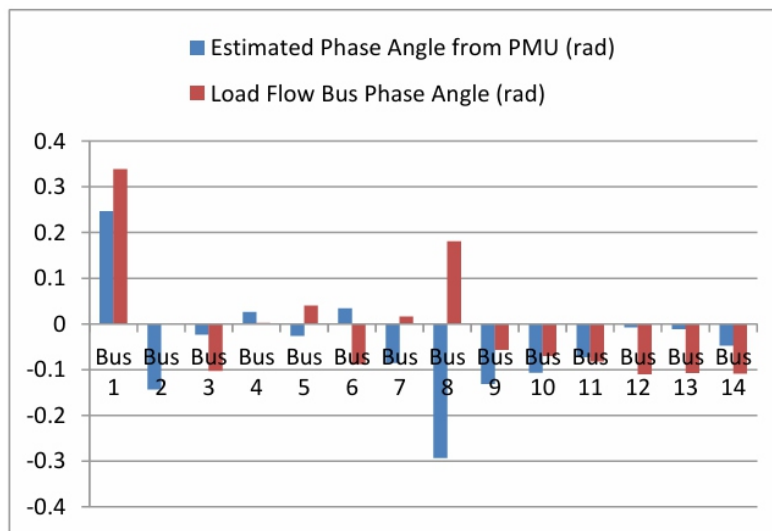


Figure 7b: Phase angle values for load flow analysis and PMUs for IEEE 14 bus

Table 1: comparison of proposed method (graph theoretic procedure) with previous methods for optimal placement of PMU on IEEE 14 – Bus Network.

Network	Method	Number of PMUs	Bus Location of PMUs
IEEE 14-Bus Network	Proposed Method	5	1,4,6,10,14
	Depth first Algorithm	6	1,4,6,8,10,14
	Genetic Algorithm (GA)	4	2,7,10,13
	Integer Linear Programming (ILP)	4	2,6,7,9
	Artificial Bee Colony (ABC) Algorithm	4	2,7,11,13

Table 2: PMUs Bus location using Proposed Method on IEEE 33-Bus network

Network	Method	Number of PMUs	Bus Location of PMUs
IEEE 33 – Bus Network	Proposed Method	14	1,3,6,9,11,13,15,17,19,21, 24,28,30,32.

Conclusion

This research work explores the capability of graph theoretic procedure method to optimally site PMU on electric power network with the PMUs voltage magnitude and phase angle measurement in real-time. This method was tested on IEEE 14- Bus and IEEE 33- Bus network. For IEEE 14-Bus network, 5 PMUs was installed on the network and was able to observe the whole network while 14 PMUs were required to fully observed IEEE 33-Bus Network. The PMUs measured voltage magnitude and phase angle were compared with the load flow analysis using newton Raphson Method.

References

- [1] M. Ravindra, R. Srinivasa Rao, A. Ramesh, and K. M. K. Reddy, "Critical bus ranking constrained optimal allocation of PMUs for network observability," *Mater. Today Proc.*, no. xxxx, 2021, doi: 10.1016/j.matpr.2021.03.376.
- [2] P. M. Joshi and H. K. Verma, "Synchrophasor measurement applications and optimal PMU placement: A review," *Electr. Power Syst. Res.*, vol. 199, no. June, p. 107428, 2021, doi: 10.1016/j.epsr.2021.107428.
- [3] K. Satish Kumar and M. Sydulu, *Optimal PMU placement techniques for the topological observability of a partial network of the southern grid of India*, vol. 3, no. PART 1. IFAC, 2014.
- [4] M. Zare, R. Azizipanah-Abarghooee, M. Malekpour, and V. Terzija, *Optimal PMU placement framework under observability redundancy and contingency—an evolutionary algorithm using DIgSILENT programming language module*, vol. 0, no. 9783319505312. 2018.
- [5] J. Pan, A. Dong, J. Fan, and Y. Li, "Online Static Voltage Stability Monitoring for Power Systems Using PMU Data," *Math. Probl. Eng.*, vol. 2020, 2020, doi: 10.1155/2020/6667842.
- [6] M. Dehghani, B. Shayanfar, and A. R. Khayatian, "PMU ranking based on singular value decomposition of dynamic stability matrix," *IEEE Trans. Power Syst.*, vol. 28, no. 3, pp. 2263–2270, 2013, doi: 10.1109/TPWRS.2013.2246196.
- [7] I. Kamwa, A. K. Pradhan, G. Joos, and S. R. Samantaray, "Fuzzy partitioning of a real power system for dynamic vulnerability assessment," *IEEE Trans. Power Syst.*, vol. 24, no. 3, pp. 1356–1365, 2009, doi: 10.1109/TPWRS.2009.2021225.
- [8] E. O. Okendo, C. W. Wekesa, and M. J. Saulo, "Optimal placement of Phasor Measurement Unit considering System Observability Redundancy Index: case study of the Kenya power transmission network," *Heliyon*, vol. 7, no. 7, p. e07670, 2021, doi: 10.1016/j.heliyon.2021.e07670.
- [9] O. Ciniglio, M. Papic, M. Vaiman, and M. Vaiman, "Optimal PMU placement to achieve complete observability of Idaho Power Co. System," *2017 IEEE Power Energy Soc. Innov. Smart Grid Technol. Conf. ISGT 2017*, pp. 1–5, 2017, doi: 10.1109/ISGT.2017.8085995.
- [10] A. El-Zonkoly, S. El-Safty, and R. Maher, "Optimal placement of PMUs using improved tabu search for complete observability and out-of-step prediction," *Turkish J. Electr. Eng. Comput. Sci.*, vol. 21, no. 5, pp. 1376–1393, 2013, doi: 10.3906/elk-1105-51.
- [11] M. Esmaili, K. Gharani, and H. A. Shayanfar, "Redundant observability PMU placement in the presence of flow measurements considering contingencies," *IEEE Trans. Power Syst.*, vol. 28, no. 4, pp. 37653773, 2013, doi: 10.1109/TPWRS.2013.2257883.

- [12] H. H. Müller and C. A. Castro, "Genetic algorithm-based phasor measurement unit placement method considering observability and security criteria," *IET Gener. Transm. Distrib.*, vol. 10, no. 1, pp. 270–280, 2016, doi: 10.1049/iet-gtd.2015.1005.
- [13] J. Peng, Y. Sun, and H. F. Wang, "Optimal PMU placement for full network observability using Tabu search algorithm," vol. 28, pp. 223–231, 2006, doi: 10.1016/j.ijepes.2005.05.005.
- [14] S. Member and S. Member, "Multiple Solutions of Optimal PMU Placement Using Exponential Binary PSO Algorithm for Smart Grid Applications Tapas Kumar Maji Parimal Acharjee," vol. 9994, no. c, 2017, doi: 10.1109/TIA.2017.2666091.
- [15] A. Ahmadi, Y. Alinejad-beromi, and M. Moradi, "Expert Systems with Applications Optimal PMU placement for power system observability using binary particle swarm optimization and considering measurement redundancy," *Expert Syst. Appl.*, vol. 38, no. 6, pp. 7263–7269, 2011, doi: 10.1016/j.eswa.2010.12.025.
- [16] V. K. Jadoun and A. Agarwal, "Latest Trends in PMU Placement Techniques," no. June, 2020, doi: 10.1109/PARC49193.2020.236622.
- [17] S. Chatterjee and S. Mandal, "A novel comparison of gauss-seidel and Newton- raphson methods for load flow analysis," *Int. Conf. Power Embed. Drive Control. ICPEDC 2017*, pp. 1–7, 2017, doi: 10.1109/ICPEDC.2017.8081050.
- [18] H. Le Nguyen, "Newton-raphson method in complex form," *IEEE Trans. Power Syst.*, vol. 12, no. 3, pp. 1355–1359, 1997, doi: 10.1109/59.630481.
- [19] G. N. Korres, P. J. Katsikas, K. A. Clements, and P. W. Davis, "Numerical Observability Analysis Based on Network Graph Theory," vol. 18, no. 3, pp. 1035–1045, 2003.
- [20] R. Sen Biswas, A. Pal, T. Werho, and V. Vittal, "A Graph Theoretic Approach to Power System Vulnerability Identification," *IEEE Trans. Power Syst.*, vol. 36, no. 2, pp. 923–935, 2021, doi: 10.1109/TPWRS.2020.3010476.
- [21] B. R. Bhowmik, "Studies on Dimultigraph and Prograph Based Applications of Graph Theory in Computer Science," no. May, 2014, doi: 10.47893/IJCCT.2010.1039.

MECHANICAL PROPERTIES OF DRAMIX HOOKED END STEEL FIBER REINFORCED CONCRETE

Falmata A. Mustapha
Department of Civil Engineering Technology,
Federal Polytechnic Damaturu, 620221, Yobe State, Nigeria
* famata1241@gmail.com

ABSTRACT

Concrete and other cementitious materials are renowned for their poor tensile strength and brittle failure. One of the best ways to combat the brittleness of cementitious materials is by using steel fibres. This research aims to provide knowledge on the properties of steel fibre-reinforced concrete. The research will focus mainly on the mechanical properties of concrete reinforced with Dramix hooked-end steel fibre with different proportions of 0%, 0.5%, 1%, 1.5%, and 2%. The evaluation of concrete properties will include the workability of concrete using a slump test, compressive strength test, splitting tensile test, and flexural strength test at the age of 7 and 28 days of curing. The slump values of steel fibre reinforced concrete (SFRC) are lower to the tune of 1.74 – 6.97 %. There is an increase in compressive strength of SFRC from 4.37% - 15.11%. The maximum increase in splitting tensile strength of 15% was obtained at a steel fibre volume fraction of 2.0%. The addition of steel fibres significantly improves the mechanical properties of concrete. A 2% volume of steel fibre is recommended as the optimum steel fibre content in concrete for practical applications.

Keywords: Concrete, Steel Fiber, Compressive strength, Tensile Strength, Flexural Strength

Introduction

One of the most frequently utilized building materials worldwide is concrete. The number of infrastructures, such as buildings, structures, highways, and railroads, has increased recently, and so the needs for concrete. Concrete is in higher demand, which has led to increased performance criteria. Additional requirements for concrete are also put forth by environmental protection and energy conservation laws. Furthermore, concrete exhibits poor tensile and strain endurance, brittle failure, and is a semi-brittle material. Typically, the tensile strength of a material is 8–15% of its compressive strength (Mahmud, 2022). To increase tensile strength and ductility, reinforcement, such as steel bars or fibres, is used to enhance ductility and tensile strength (Banthia and Sappakittipakorn, 2007). Concrete reinforced with steel fibres has improved energy absorption, deformation before failure, and ductile behaviour as a result of the incorporation of steel fibres (Islam et al., 2021).

Before cement was invented, the Egyptian and Babylonian civilizations employed steel fibres to reinforce brittle materials (A. A. Shah and Ribakov, 2011). It is generally known that steel fibres' primary function is to reinforce concrete by bridging cracks as they form and enhancing its ductility. Steel fibre-reinforced concrete has more energy absorption capacity due to the inclusion of fibres, which also increase strain at peak load. It has been shown that steel fibres also significantly increase the concrete's impact resistance, tensile resistance, ductility, and static flexibility (Mohammadi et al., 2008).

Furthermore, steel fibre improves concrete's tensile strength and flexural properties, which are regarded as the material's major structural weaknesses (Lee, 2017; Mahmud, 2022). There are several uses for fibre-reinforced concrete, including buildings, tunnels, and bridges. The influence of steel fibres on concrete has been the subject of numerous studies over the past few decades. Steel fibres' mechanical properties can be improved by using deformed fibres like hooked fibres. Theoretically, compared to other forms of fibre, fibres with hooked ends offer higher mechanical coupling (Boulekbache et al., 2016).

In general, increasing fibre volume can improve mechanical qualities. This is due to the rise in fibre usage to support loads (Z. Wu et al., 2019). Despite a decrease in flowability, Wu et al. (2019) showed that adding around 3% more fibre to SFRC enhanced its compressive and flexural properties when mixed with a consistent superplasticizer (SP) dosage. According to Shi et al., (2016), concrete with 2% steel fibre is much more dependable than concrete with 1% or 3% steel fibre, and 2% is the optimal fibre level for SFRC. The impact of steel fibres on the rheological characteristics, flexural toughness, flexural strength, splitting tensile and compressive strength of self-compacting concrete (SCC) was examined by Khaloo et al., (2014). The findings showed that employing large percentages of fibres resulted in a loss in various rheological properties that have been stipulated by EFNARC and ACI 237R, which in turn influenced the workability of medium and high-strength SCC classes. Similar findings were reported by Li et al., (2017) which showed that adding steel fibres greatly reduced the workability of freshly produced concrete. The following reasons might be given for the decline in slump value: (i) The networks of randomly positioned fibres reduced the workability of freshly mixed concrete; (ii) Since the fibres had a big surface area, they required a lot of cement paste to wrap it, thus, increasing the viscosity of the freshly mixed concrete mixes. According to Mohammadi et al., (2008), the compressive strength increases as the proportion of short fibres in the concrete mix as well as the gross fibre content of the mixture rises.

In the study by Chen and Carson (1971), the concrete mixes with shorter fibres showed better compressive strengths than those with longer fibres for a given volume fraction of fibres. In the research of Shah and Rangan (1971), the addition of fibres to concrete increased compressive strength by up to 23%. According to a study by Khaloo et al., (2014), fibre volume fractions have an impact on the splitting tensile strength, with higher fibre fractions increasing splitting tensile strength. The SCC specimens' splitting tensile strength was improved by the inclusion of steel fibres. By spanning the space between the two sides of the crack opening, steel fibres increase the splitting tensile strength. For the medium and high-strength plain specimens, the inclusion of a 2% fibre volume fraction increased splitting tensile strength by 28.5% and 17.1%, respectively. A key indicator that can indicate the toughening effects of fibres and the interior structural performance of matrices is flexural toughness. Furthermore, Lin et al., (2014) examined the impact of fibre types on the flexural properties of self-compacting fibre-reinforced cementitious composites and found that these factors had a minimal bearing on specimens' initial crack strength and pre-cracking behaviour. However, fibre properties had a big impact on post-cracking behaviour and deflection types (deflection-hardening or deflection-softening). Additionally, Wu et al., (2016) investigated how the amount and shape of steel fibres (SF) influenced the flexural properties of ultra-high performance concrete (UHPC). The scientists found that whereas SF concentration had a significant impact on peak load, it had minimal impact on first crack strength and the corresponding deflection of UHPC. The findings from Deng et al., (2016) showed that increasing fibre length, fibre content, and concrete strength considerably improved the postcracking behaviour of fibre-reinforced concrete (FRC). Comparable to this, Khaloo et al., (2014) find that the use of steel fibres increased the

flexural strength.

Further research has shown that adding steel fibres to concrete enhances its flexure and impact strength. Song, and Hwang (2004) assessed the effect of fibre on the compressive resistance of concrete in terms of the fibre-reinforcing factor. They have discovered that while high-strength concrete has weak tensile resistance and strain capacities, adding steel fibres to it can make it less brittle. Rai and Joshi (2014) did a study on the properties and usage of SFRC. Their study revealed that the use of fibre boosts concrete's ductility and ability to withstand loads after cracking. Concrete that has fibres added to it is more resistant to bending and can absorb energy after the initial break (Abaza, 2014). Vega (2016) noted that the use of fibres aids in reducing the thickness of the structural elements because it avoids the use of minimal coatings to ensure the integrity of the reinforcement and the different fibres better sew the concrete matrix, which results in better control of cracks and increases the durability of the material. Researchers discovered that steel fibres may greatly improve post-cracking energy absorption properties as well as toughness (Fantilli et al., 2011; Marar et al., 2011) but also lead to a greater compressive (Lu and Hsu, 2006), flexural (Ding and Liu, 2010) and tensile strength (Grimaldi and Luciano, 2000) of concrete. Concrete's brittleness has been effectively reduced by the use of steel fibres. Similar to straw in mud, steel fibres may span concrete fissures and prevent them from spreading, giving the concrete a post-crack behaviour.

This study examines the mechanical characteristics of Dramix hooked-end steel fibre reinforced concrete with various steel fibre contents of 0%, 0.5%, 1%, 1.5%, and 2% to enhance concrete performance. The characteristics of steel fibre-reinforced concrete will be experimentally investigated in both the fresh and hardened states. The workability of concrete will be assessed using a slump test as part of the assessment of fresh properties. Whereas the hardened properties of the concrete comprise the compressive strength test, splitting tensile test, and flexural strength test. Based on the findings of the study's results, the optimal steel fibre content to be employed will be chosen.

Materials and Methods

Cement

The concrete mixes were made using ordinary Portland Cement of CEM 1 with a strength of 42.5 MPa and a specific gravity of 3.15. The chemical composition of the cement utilized is presented in Table 1.

Fine and Coarse aggregates

Natural river sand with relative densities of 2.65 kg/m³, 1.15% water absorption, and 3.17 in terms of fineness modulus were employed for the mixes. A well-graded 10 mm aggregate with a relative density (SSD) and water absorption value of 2.66 kg/m³ and 1.0%, respectively, was utilized as coarse aggregate, according to BS 882 (1992).

Table 1. Chemical Composition of Portland Cement

Component	SiO ₂	Al ₂ O ₃	Fe ₂ O ₃	CaO	MgO	SO ₃	K ₂ O	Na ₂ O	Ignition Loss
Weight (%)	20.60	4.80	2.90	63.60	2.50	3.20	1.10	0.40	0.07

Steel Fibers

Four different volume fractions of Dramix Hooked-end section circular steel fibre were used: 0.5%, 1%, 1.5%, and 2%. The steel fibres utilized were Dramix hooked-end steel fibres, BN type RC 65/35, with

dimensions of 35 mm in length, 65 in aspect ratio, 7850 kg/m³ in density, and 1250 MPa in tensile strength. The physical appearance of the Hooked-end steel fibre is shown in Figure 1. It has been proven that steel fibre with hooks at one end will help the fibre and concrete matrix bind appropriately. Additionally, the binding is dependent on the mechanical interlocks created by the hooks of the fibres in addition to chemical adhesion and static friction (Abdallah et al., 2018).

Mixture Proportions and Specimen Preparation

Table 2 displays the mixture proportion for the steel fibre-reinforced concrete (SFRC) employed in this experiment. The water-to-cement ratio in the concrete is 0.48. No water-reducing additives were used. Hooked-end steel fibres having a density of 7850 kg/m³ were employed in five different ratios: 0%, 0.5%, 1%, 1.5%, and 2% by volume fraction. The laboratory investigation consisted of tests for both fresh and hardened concrete properties.

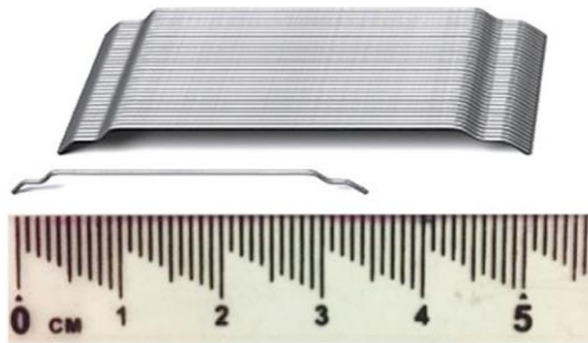


Figure 1. Dramix hooked end section of circular steel fibre

Table 2. Mixture Proportion of SFRC

Volume Fraction	Cement (kg/m ³)	Fine Aggregate (kg/m ³)	Coarse Aggregate (kg/m ³)	Water (kg/m ³)	Hooked-end Steel Fiber (kg/m ³)
0%	400	651	1087	192	0
0.5%	400	651	1087	192	39
1.0%	400	651	1087	192	78
1.5%	400	651	1087	192	118
2.0%	400	651	1087	192	157

A consistent SFRC blend was made by three different rounds of fibre mixing. The top of the mould was cleaned of excess material, and the surface was trowelled smoothly. After 24 hours, the samples were demolded, and they were left to cure at room temperature until testing age.

Slump Test

The workability of concrete will be assessed using a slump test as part of the assessment of the fresh properties. For the workability of SFRC, ACI Committee 544 suggested using an inverted slump cone test (ACI544.2R-89, 2009). According to the ACI manual of concrete practice, the workability of the fresh concrete mix is its capacity to adequately fill the form or mould with the necessary work (vibration) while maintaining the quality of the concrete. The broad end of the cone should be facing down on a flat, nonabsorptive surface. Then, it is filled in three equal levels, each of which is tamped with a steel rod to

compact the layer (ASTMC143/C143M-10a, 2010). The encased material will slump somewhat owing to gravity when the cone is carefully taken off, as illustrated in Figure 2.



Figure 2. Slump Test

Hardened Properties Test

The hardened properties test on the concrete comprises:

Compressive Strength Test

According to BS EN12390-3 (2009), a 3000 kN capacity universal testing equipment was used to perform the compressive strength test on 100×100 mm cubes, as depicted in Figure 3. The test was conducted at the ages of 7 and 28 days. For each batch, three (3) samples were tested, and the average value was computed to determine the compressive strength by applying Equation 1.

$$F_c = F/A_c \quad \text{Eqn. (1)}$$

Where; F_{ct} is the splitting tensile strength in MPa, F is the maximum load in Newton, L is the height of the sample in mm, and D is the diameter of the specimen in mm.

Flexural Strength Test

According to BS EN 12390-5 (2009), a flexural strength test on a $100 \times 100 \times 500$ mm prism was conducted at 7 and 28 days after curing. By applying force through the top and lower rollers, the sample is subjected to a four-point bending test. Up to 20% of the failure load was applied as the initial load during testing. After the initial load was applied, the load was maintained at a constant rate of 0.04 N/mm² until sample failure.



Figure 3. Compressive strength test on Concrete cube samples



Figure 4. Flexural Strength Test

The flexural strength was then calculated by using Equation 3.

$$f_{ct} = \frac{P \times I}{d_1 \times d_2^2} \quad \text{Eqn. (3)}$$

Where ‘P’ is the maximum applied load (N), ‘I’ is the distance between the supporting rollers (mm), d1 is the width of specimen (mm) and d2 is the depth of specimen (mm).

Results and Discussions

Fresh Concrete

Following the addition of 2% steel fibre to the concrete, workability decreased. The findings of the slump test shown in Figure 5 indicate that concrete reinforced with steel fibres has lower slump values than reference concrete. In comparison to the reference concrete, the findings reveal a slump value reduction of 1.74 to 6.97%. As the steel-fibre ratio rises, the slump value decreases as well. Parallel to this, Köroğlu (2018) also noted that when the amount of steel fibre in concrete increases, the slump value decreases.

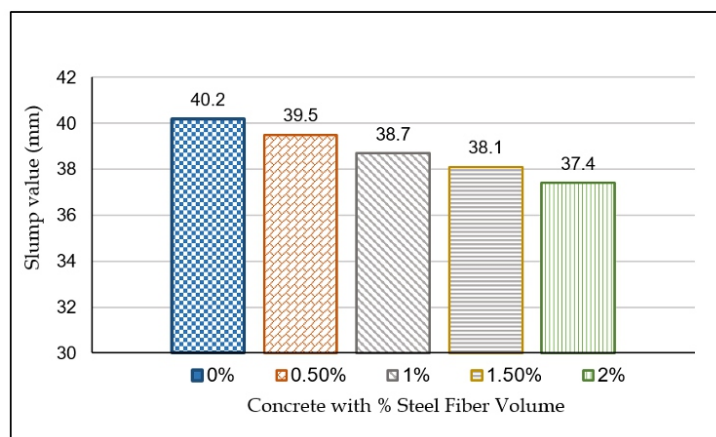


Figure 5. Slump Value of Steel Fiber Reinforced Concrete

The workability of concrete may be affected by steel fibre. The coarse aggregate movement is prevented by the fibres, which lessens the material's flexibility. An increase in the mortar composition and/or the

initial slump might lessen such impact and create ideal working conditions (Figueiredo et al., 2015). Superplasticizers and other high-range water-reducing admixtures should always be used in SFRC. Lowlevel fibre addition minimizes fibre balling and creates concrete with homogenous material consistency and excellent workability (Song and Hwang, 2004). Thus, considering the experimental test results, a 2% volume of fibre is recommended as the optimum fibre context for practical applications. A recommendation of 2% was used in many studies (Aksoylu et al., 2022; Zeybek et al., 2022).

Hardened Properties of SFRC

The properties considered in this section are compressive strength, splitting tensile strength, and flexural strength.

Compressive strength of SFRC

Figure 6 displays the results of compressive strength tests on reference concrete and SFRC with various fibre volume fractions for a curing age of 7 and 28 days. It is clear that when the fraction of fibres rises, the compressive strength increases as well. According to the findings, adding fibres to concrete at a curing age of seven days often increases compressive strength ranging from 3.96% to 19.75%, as shown in Figure 6. Additionally, it can be seen that at a curing age of 28 days, concrete with 0.5%, 1.0%, 1.5%, and 2.0% volume fractions of fibres increases its compressive strength by 4.37%, 6.63%, 12.57%, and 15.11%, respectively. This can be due to the presence of steel fibre, which primarily works to prevent fractures from forming. Therefore, the steel fibres' major role is mostly as a crack preventer rather than in actual compression (Majain et al., 2019). Furthermore, there is an optimal volume proportion of fibres for a given mix that provides the highest strength, and this is 2.0%.

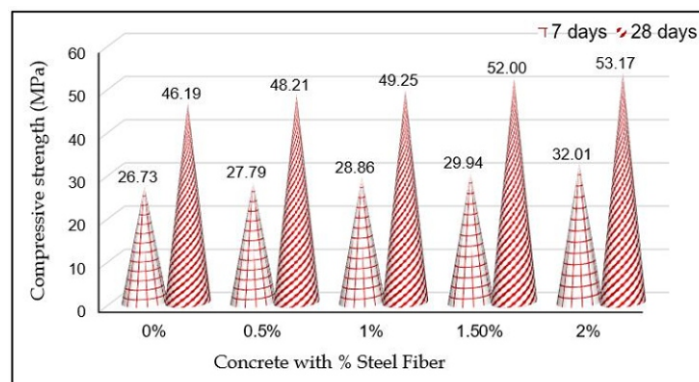


Figure 6. Compressive Strength of SFRC

In general, it can be deduced that the compressive strength increases as the amount of steel fibre in the mixture raises. According to Mohammadi et al., (2008), the compressive strength improves with an increase in the proportion of short fibres in concrete mix and an increase in the gross fibre content in the mix. Likewise, Shah and Rangan (1971) stated that the addition of steel fibres to concrete increased compressive strength by up to 23%.

Splitting Tensile Strength of SFRC

The splitting tensile strength test was performed to find the capacity of SFRC in tension, which is an important mechanical parameter for concrete performance. Figure 7 depicts the impact of steel fibre on the concrete's splitting tensile strength at 7 and 28 days after curing. Figure 7 makes it clear that the inclusion of steel fibre increases the splitting tensile strength of the concrete in comparison to the reference concrete.

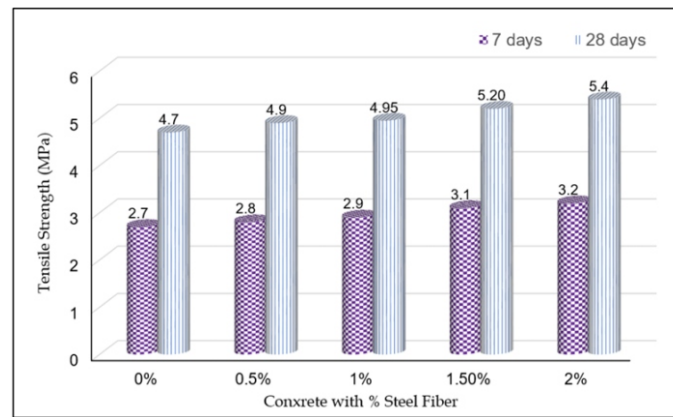


Figure 7. Tensile Strength of SFRC

The 28-day findings revealed an increase in tensile strength of 4.26%, 5.32%, 10.64%, and 14.89% for concrete mixes containing volume fractions of steel fibre of 0.5%, 1.0%, 1.5%, and 2.0%, respectively. At a steel fibre volume percentage of 2.0%, a maximum improvement in splitting tensile strength of 15% over reference concrete was noted. The SF's bridging effect across the fracture is what causes the increase in tensile strength, which in turn prevents the crack from spreading and enlarging (Grimaldi and Luciano, 2000).

Flexural Strength of SFRC

The flexural strength of the SFRC beam is improved by the inclusion of steel fibre as depicted in figure 8. In comparison to the reference concrete, which had a flexural strength of 4.63 MPa, the SFRC beam's flexural strength was 8.98 MPa for 2% steel fibre volume. The engineering properties of concrete are considerably improved by the inclusion of steel fibres.

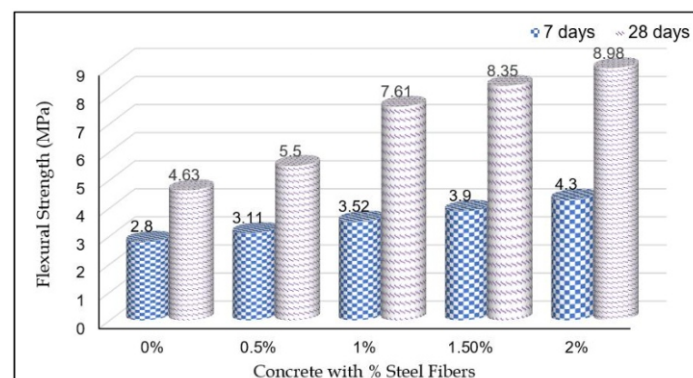


Figure 8. Mean Flexural Strength of SFRC

The 7-day flexural strength of the SFRC is accompanied by a 54% increase in strength compared to the reference concrete at 2% steel Fiber, demonstrating that the SFRC has increased flexural strength and can withstand higher loads. Additionally, the results at 28 days show that the SFRC's flexural strength was increased by 94% when compared to reference concrete containing 2% steel fibre. Salihu and Mallum, (2020) have provided documentation of a comparable finding. According to the findings, adding steel fibre to concrete caused a positive growth in the flexural strength of the concrete.

Conclusion

This paper highlights the mechanical properties of Dramix hooked-end steel fibre reinforced concrete with different proportions of steel fibre of 0%, 0.5%, 1%, 1.5%, and 2%. Based on the findings from the experiments, the following conclusions were outlined:

- The slump values of concrete with steel fibres are lower to the tune of 1.74 – 6.97 % compared to the reference concrete. Steel fibres act as a barrier to coarse aggregate movement reducing the flexibility of the material.
- There is an increase in compressive strength of SFRC from 4.37% - 15.11%. It may be concluded that with an increase in the volume fraction of steel fibre in the mix, the compressive strength improves.
- The maximum increase in splitting tensile strength of 15% with respect to reference concrete was obtained at a steel fibre volume fraction of 2.0%. The increase in tensile strength is due to the bridging action of SF across the crack, which controls the crack widening and propagation.
- The flexural strength of SFRC improves by 94% compared to reference concrete at 2% steel fibre content.
- The addition of steel fibres significantly improves the mechanical properties of concrete.
- Thus, based on the experimental test results, a 2% volume of steel fibre is recommended as the optimum steel fibre content in concrete for practical applications.

References

1. Abaza, O. (2014). *Flexural behavior of flat-end steel-fiber-reinforced concrete*. *Journal of Materials in Civil Engineering*, 8(26). [https://doi.org/10.1061/\(ASCE\)MT.1943-5533.0001015](https://doi.org/10.1061/(ASCE)MT.1943-5533.0001015)
2. Abdallah, S., Fan, M., and Rees, D. W. A. (2018). *Bonding Mechanisms and Strength of Steel Fiber Reinforced Cementitious Composites: Overview*. *Journal of Materials in Civil Engineering*, 30(3), 115. [https://doi.org/10.1061/\(asce\)mt.1943-5533.0002154](https://doi.org/10.1061/(asce)mt.1943-5533.0002154)
3. ACI 544.2R-89. (2009). *Measurement of properties of fiber reinforced concrete*.
4. Aksoylu, C., Özkılıç, Y. O., Hadzima-Nyarko, M., Işık, E., and Arslan, M. H. J. S. (2022). *Investigation on improvement in shear performance of reinforced-concrete beams produced with recycled steel wires from waste tires*. *Sustainability*, 14. <https://doi.org/10.3390/su142013360>
5. ASTM C469. (2002). *Standard Test Method for Splitting Tensile Strength of Cylindrical Concrete Specimens*, *Annual Book of ASTM Standards*. West Conshohocken; Pa, USA.
6. ASTM C143/C143M-10a. (2010). *Standard test method for slump of hydraulic-cement concrete*.
7. Banthia, N., and Sappakittipakorn, M. (2007). *Toughness enhancement in steel fiber reinforced concrete through fiber hybridization*. *Cem. Concr. Res.*, 37(9).
8. Boulekbache, B., Hamrat, M., Chemrouk, M., and Amziane, S. (2016). *Flexural behaviour of steel fibre-reinforced concrete under cyclic loading*. *Constr. Build. Mater.*, 126, 253–262.
9. British Standards Institution BSI. (1992). *Specification for aggregates from natural sources for concrete*. Bs 882-2., 1–14. <https://doi.org/10.3403/02522741>
10. BS EN 12390-2. (2009). *British Standard Institute*.
11. BS EN 12390-3. (2009). *Testing hardened concrete: Part 3, Compressive strength of test specimens*.
12. Chen, W. F., and Carson, J. L. (1971). *Stress–strain properties of random wire reinforced concrete*. *ACI Journal*, 68(12), 797–804.
13. Deng, Z. C., Shi, F., Yin, S., and Tuladhar, R. (2016). *Characterisation of macro polyolefin fibre reinforcement in concrete through round determinate panel test*. *Constr. Build. Mater.*, 121, 229–235.
14. Ding, Y. N., and Liu, S. G. (2010). *Study of the flexural and shear toughness of steel fiber reinforced self-compacting concrete*. *Chin. Civil Eng. J.*, 43(11), 55–63.

15. Fantilli, A. P., Vallini, P., and Chiaia, B. (2011). Ductility of fiber-reinforced self-consolidating concrete under multi-axial compression. *Cem. Concr. Compos.*, 33(4), 520–527.
16. Figueiredo, A. D. De, Ceccato, M. R., Jacob, R., and Steinberg, B. (2015). Workability Analysis of Steel Fiber Reinforced Concrete Using Slump and Ve-Be Test. *Materials Research*, 18(6), 1284–1290.
17. Grimaldi, A., and Luciano, R. (2000). Tensile stiffness and strength of fiber-reinforced concrete. *J. Mech. Phys. Solids*, 48(9), 1987–2008.
18. Islam, A., Shuvo, A. K., Chowdhury, S. A., Sharmin, S., and Hasan, M. (2021). A Comparative Study on the Properties of Natural, Synthetic and Steel Fibre Reinforced Concrete. *J. Civ. Eng. Constr.*, 10(4), 216–224.
19. Khaloo, A., Raisi, E. M., Hosseini, P., and Tahsiri, H. (2014). Mechanical performance of selfcompacting concrete reinforced with steel fibers. *Construction and Building Materials*, 51, 179–186. <https://doi.org/10.1016/j.conbuildmat.2013.10.054>
20. Koroğlu, M. A. (2018). Behavior of composite self-compacting concrete (SCC) reinforced with steel wires from waste tires. *Revista de Construcción J. Constr.*, 17, 484–498.
21. Lee, J. H. (2017). Influence of concrete strength combined with fiber content in the residual flexural strengths of fiber reinforced concrete. *Compos. Struct.*, 168, 216–225,. <https://doi.org/10.1016/j.compstruct.2017.01.052>.
22. Li, J. J., Wan, C. J., Niu, J. G., Wu, L. F., and Wu, Y. C. (2017). Investigation on flexural toughness evaluation method of steel fiber reinforced lightweight aggregate concrete. *Construction and Building Materials*, 131, 449–458. <https://doi.org/10.1016/j.conbuildmat.2016.11.101>
23. Lin, C., Kayali, O., Morozov, E. V., and Sharp, D. J. (2014). Influence of fibre type on flexural behaviour of self-compacting fibre reinforced cementitious composites. *Cem. Concr. Compos.*, 51, 2737.
24. Lu, X. B., and Hsu, C. T. (2006). Behavior of high strength concrete with and without steel fiber reinforcement in triaxial compression. *Cem. Concr. Res.*, 36(9), 1679–1685.
25. Mahmud, J. Al. (2022). Effect of the Inclination Angle of Hooked Steel Fiber on the Flexural Behavior of Steel Fiber Reinforced. In *6th International Conference on Advances in Civil Engineering (ICACE2022)* (pp. 0–9).
26. Majain, N., Rahman, A. B. A., Mohamed, R. N., and Adnan, A. (2019). Effect of steel fibers on selfcompacting concrete slump flow and compressive strength. *IOP Conference Series: Materials Science and Engineering*, 513(1). <https://doi.org/10.1088/1757-899X/513/1/012007>
27. Marar, K., Eren, O., and Celik, T. (2011). Relationship between impact energy and compression toughness energy of high-strength fiber-reinforced concrete. *Mater. Lett.*, 47(4–5), 297–304.
28. Mohammadi, Y., Singh, S. P., and Kaushik, S. K. (2008). Properties of steel fibrous concrete containing mixed fibres in fresh and hardened state. *Construction and Building Materials*, 22, 956–965. <https://doi.org/10.1016/j.conbuildmat.2006.12.004>
29. Rai, A., and Joshi, Y. P. (2014). Applications and properties of fibre reinforced concrete. *Int. Journal of Engineering Research and Applications*, 4(5), 123–131.
30. Salihu, K., and Mallum, I. S. A. (2020). MECHANICAL PROPERTIES OF STEEL FIBRE REINFORCED CONCRETE. *International Journal of Civil, Structural, Environmental and Infrastructure Engineering Research and Development (IJCSEIERD)*, 10(3), 9–18.
31. Shah, A. A., and Ribakov, Y. (2011). Recent trends in steel fibered high-strength concrete. *Materials and Design*, 32(8–9), 4122–4151. <https://doi.org/10.1016/j.matdes.2011.03.030>
32. Shah, S. P., and Rangan, B. V. (1971). Fibre reinforced concrete properties. *ACI Journal*, 68(2), 12635.
33. Shi, C., He, W., and Wu, L. (2016). Effects of steel fiber content and shape on mechanical properties of ultra high performance concrete. *Constr. Build. Mater.*, 103, 8–14.

-
34. Song, P. S., and Hwang, S. (2004). *Mechanical properties of high-strength steel fiberreinforced concrete*. *Construction and Building Materials*, 18(9), 669–673.
35. Vega, G. (2016). *Review of the steel fibers use in concrete*. *Anales de Edificación*, 2(3), 41–51. <https://doi.org/10.20868/ade.2016.3471>
36. Wu, Z. M., Shi, C. J., He, W., and Wu, L. M. (2016). *Effects of steel fiber content and shape on mechanical properties of ultra high performance concrete*. *Constr. Build. Mater.*, 103, 8–14.
37. Wu, Z., Shi, C., and Khayat, K. H. (2019). *Investigation of mechanical properties and shrinkage of ultra-high performance concrete: Influence of steel fiber content and shape*. *Compos. Part B Eng.*, 174. <https://doi.org/10.1016/j.compositesb.2019.107021>
38. Zeybek, Ö., Özkılıç, Y. O., Çelik, A. İ., Deifalla, A. F., Ahmad, M., and Sabri Sabri, M. M. (2022). *Performance evaluation of fiber-reinforced concrete produced with steel fibers extracted from waste tire*. *Frontiers in Materials*, 9(November). <https://doi.org/10.3389/fmats.2022.1057128>.

EVALUATING THE FLEXURAL STRENGTH OF CORRODED REINFORCED CONCRETE BEAMS

Ibim Green
Kelechi Ugoji

ABSTRACT

Corrosion of reinforcing steel is one of the most deterioration factors that influence reinforced concrete structures. Quantifying the effect of corrosion before structural failure is significant for a cheaper and more efficient repair. In this paper, a simple model was used to predict the residual flexural strength of RC beams with varying degrees of reinforcement corrosion based on experimental results. The Model was developed from analysing several beam specimens available in literature, which have been damaged by accelerated corrosion. The validity of this study was compared with separate set of published data. The new proposed model in this study was able to successfully predict the residual flexural strength of corroded reinforced concrete beams. It is recommended to study in future work the applicability of this model to full-scale RC beams that underwent natural corrosion or failed in flexure by concrete crushing.

Keywords: Serviceability, Reinforced Concrete, Corrosion, Flexural strength, Analysis of Variance

Introduction

Corrosion of steel reinforcement is one of the most predominant causes of the deterioration of reinforced concrete (RC) structures, greatly shortening the service life of the structure and increasing maintenance costs (Bertolini et al. 2004). The corrosion of reinforcement causes a decrease in rebar diameter, cracking and spalling of the concrete cover, which adversely affects the ultimate strength of RC structures. Furthermore, when the steel rebar corrodes, the corrosion products of reinforcing steel exert stresses within the concrete resulting in the formation of cracks along the reinforcing bars. These cracks weaken the bond and the anchorage between steel and concrete and lead to cracking and spalling of concrete which in turn facilitates the ingress of oxygen and moisture to the reinforcing steel and increases the rate of corrosion (Berto et al., 2008). The rehabilitation of RC structures affected by corrosion costs billions of dollars every year (Imam et al. 2015). Reinforcement corrosion should thus be of great concern to engineers when designing new structures. The residual strength of old structures should be properly estimated in order to ensure that the required repairs are performed on time to guarantee public safety.

Corrosion of reinforcements involves the movement of ions or charges from the active anodic sites, where iron atoms are being dissolved, towards the passive cathodic sites, where oxygen are being consumed (Imam et al 2015). These two reactions combine to produce very soluble and expansive rust products that cause progressive damage on RC beams. For prematurely corroding structures, assessment is required to administer appropriate maintenance and repair, or provide information about their remaining service life. However, evaluation practices normally utilize destructive techniques and costly technologies that are material and labor intensive (Wang et al 2008). Predictive models provide cheaper and more convenient alternatives to these advanced corrosion assessments (Bertolini et al. 2004).

Objectives of the study

(1) To develop a model that can be used to predict the relative flexural strength of corroded concrete members. The need for the prediction of the relative strength often arises to determine the underlying safety of the corroded members and to decide when the repair or strengthening must be undertaken without any further delay.

(2) Demonstrate the validity of the proposed models by comparing the computed residual flexural strength to the actual flexural strength obtained from bending tests.

Data gathering

Data used for this model development were analyzed from literature (Imam et al 2015). Reinforced Concrete beam specimens have been gathered with general layout drawn in Fig. 1(a) to (c). Experimental investigations generally involved partially immersing the beam specimens in 3.5–5.0% NaCl solution while an external current of intensities, varying from 1 to 3 mA/cm², is being applied for periods of 4 days up to 3 weeks. Corroded samples were then tested in flexure by centerpoint (Fig. 1d) to get the residual moment capacity ($M_{ex,c}$); after which, the reinforcing bars were extracted and cleaned chemically for mass loss measurement (Broomfield 2002).

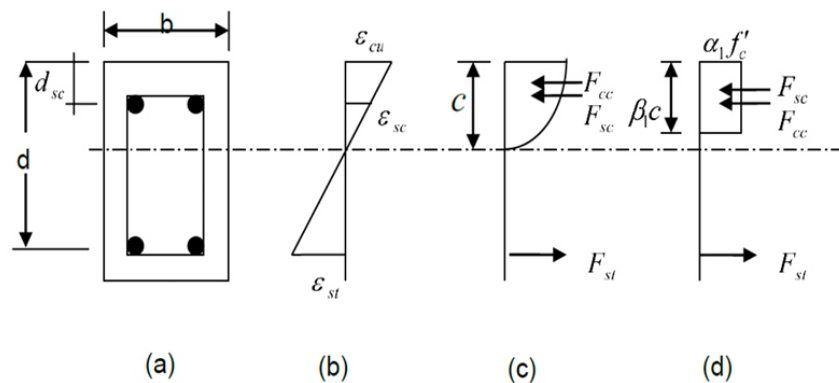


Figure 1: Vertical stress and strain distribution: (a) typical reinforced concrete beam section (b) strain distribution (c) actual concrete stresses (d) equivalent concrete stresses

The stress and strain distributions of reinforced concrete beam are shown in Fig. 1. The flexural strength of reinforced concrete beams can be calculated from Equation 1.

$$Mu = Ast * fy * (d - c) + Asc * fsc * (c - dsc) + \alpha_1 f_c \beta_1 cb * (c - \beta_1 c / 2) \quad [1]$$

Where,

MU = Ultimate moment of resistance before corrosion

fy = steel yield strength

d = depth of tensile steel reinforcement measured from top face of the beam

c = depth of neutral axis measured from the top face of the beam

fsc = steel stress in compression

Ast = area of tensile steel reinforcement

Asc = area of compression steel reinforcement

f_c = concrete compressive

dsc = depth of compression steel reinforcement

B = width of the beam

α_1 and β_1 are concrete stress block factors as shown Fig. 1.

Equation 1 can be used for uncorroded beams, however when the beams get corroded there will be a reduction in the moment resistance due to the loss of the cross sectional area of the steel and the loss of

the bond between the concrete and the steel. Therefore, Equation 1 cannot be used to determine the flexural strength of reinforced concrete beam.

Data analysis

Assuming a uniform corrosion over the surface of the reinforcing bar, and the concrete in tension is cracked and no longer contribute to the tensile resistance of RC beam; the tensile force for a beam designed to fail in bond, at any corrosion level x_p is given as follows:

$$F_{stx} = n_{st} * \pi * d_{stx} * \tau_{bu} * l_d \quad [2]$$

Where,

n_{st} = number of reinforcing bars in tension

d_{stx} = reduced diameter of reinforcing bars in tension at corrosion level x_p

τ_{bu} = bond strength of reinforcing bars in tension at corrosion level x_p

l_d = development length.

When the reinforcing bar corroded, the stress in the steel is less than the yield stress. The reason for this is that the formation of corrosion products layer exerts an outward pressure on the concrete from inside and as the pressure builds, the ultimate result is cracking of the concrete, which in turns results in a loss of bond between steel and concrete. Therefore, stresses in concrete cannot be transferred to the reinforcing steel properly. Stress in the corroded steel bar cannot be obtained from the strain compatibility equation because plain sections before bending will not remain plain after bending. Thus, the strain compatibility becomes invalid for corroded bars (Wang and Liu 2008).

From compatibility requirement as shown in Fig. 1, the strain for steel in compression can be obtained from Equation 3:

$$\varepsilon_{sc} = \varepsilon_c (c - d_{sc}) / c \quad [3]$$

Therefore, the compression force carried by steel in compression is:

$$F_{sc} = A_{sc} * E_s * \varepsilon_c (c - d_{sc}) / c \quad [4]$$

From equilibrium,

$$F_{stx} = F_{sc} + F_{cc} \quad [5]$$

The depth of neutral axis can be obtained from Equation 5, and the ultimate moment of resistance after corrosion can be determined as follows:

$$M_u = F_{stx} * (d - c) + F_{sc} * (c - d_{sc}) + F_{cc} * (c - \beta_1 c^2) \quad [6]$$

Model development

Corrosion coefficient was first evaluated from the sample beams using Eq. (5) to initially assess how it is affected by other test variables. Results suggest a noticeable decline in corrosion coefficient at higher percent mass loss (Fig. 2a) and rebar diameter

(Fig. 2b). There is also an inverse relationship between and clear cover thickness (at tension side), but at slightly lesser degree (Fig. 2c). The applied current, on the other hand, has negligible influence (Fig. 2d). Henceforth, the model considered only the contribution from the first three parameters.

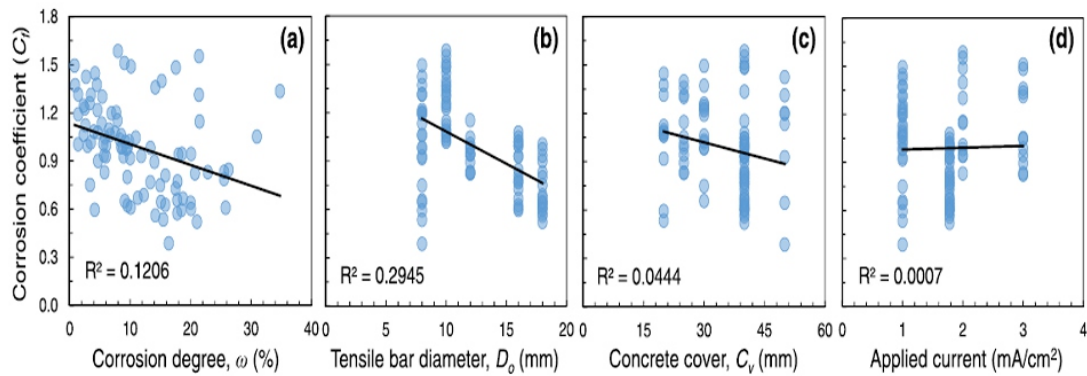


Fig. 2. Relationship between Corrosion coefficient and different RC beam parameters.

ANOVA is used in analyzing the data available (Mangat and Elgarf 1999, Rodriguez et al. 1997, Azad et al. 2007, El Maaddawy et al. 2005, Joyce 2008) to determine the residual flexural behavior of corroded reinforced concrete beams. First an interpolation of the data has been done at different levels of corrosions (Mass Loss, ML %) 2.5%, 5%, 10%, 15%, 20%, 25% and 30%. To preform that analysis, the built-in function 'anovan' in MATLAB was chosen as the primary method of variance analysis. Based on the results of ANOVA, an equation to determine the yield strength of corroded reinforcing bar as follows:

$$f_{yx} = (1 - ML/96) * f_y \quad [7]$$

Where,

f_{yx} = yield strength of corroded reinforcing bar at corrosion level x_p ,

f_y = yield strength of sound reinforcing bar

ML = mass loss percent.

The tensile force, $stx F$, at any corrosion level x_p is determined as follows:

$$F_{stx} = nst * \pi * d_{st}^2 * f_{yx}/4 \quad [8]$$

The compression force carried by steel in compression, scF , and by concrete in compression, ccF , can be obtained from Equations (4), and (5) respectively. By using the equilibrium Equation 6, the depth of neutral axis can be obtained, and the ultimate moment of resistance after corrosion can be determined from Equation 7.

Conclusions

The corrosion of steel reinforcement reduces the strength of a reinforced concrete element, thus, there is a need to predict the relative strength often arises to determine the underlying safety of the corroded RC members and to decide when the repair or strengthening must be undertaken without any further delay. In this paper, a simplified model developed based on the experimental results in the literature using ANOVA. The predicted results of the present model correlated very well with the experimental results observed in the literature.

References

1. Ahmad, S. 2017. *Prediction of residual flexural strength of corroded reinforced concrete beams. Anti Corrosion Methods and Materials* 64(1): 69-74.
2. ASCE (American Society of Civil Engineers). 2013. *Report card for America's infrastructure*. doi: <http://dx.doi.org/10.1061/9780784478837>

3. Azher, S.A. 2005. *A prediction model for the residual flexural strength of corroded reinforced concrete beams*”, M. Sc. thesis, King Fahd University of Petroleum and Minerals, Dhahran, Saudi Arabia.
4. Azad, A. K., Ahmed, S., and Azher, A. S. 2007. *Residual Strength of Corrosion-Damaged Reinforced Concrete Beams*. *ACI Material Journal* 104(1): 40-47
5. Bertolini, L., Elsener, B., Pedersen, P. and Polder, R. 2004. *Corrosion of Steel in Concrete, Prevention, Diagnosis, Repair*. Wiley-VCH Verlag GmbH and Co. KGaA, Weinheim, Germany.
6. Berto, L., Simioni, P. and Saetta, A. 2008. *Numerical modelling of bond behaviour in RC structures affected by reinforcement corrosion*. *Engineering Structures* 30: 1375-1385.
7. Broomfield, J. 2002. *Corrosion of steel in concrete: understanding, investigation and repair*. Taylor & Francis, Abingdon, UK.
8. Cabrera, J.G. 1996. *Deterioration of concrete due to reinforcement steel corrosion*. *Cement & Concrete Composites* 18(1): 47-59.
9. Canadian Infrastructure Report Card. 2016. Available from http://canadianinfrastructure.ca/downloads/Canadian_Infrastructure_Report_2016.pdf [accessed 28 February 2018]
10. El Maaddawy, T., Soudki, K., and Topper, T. 2005. *Analytical model to predict nonlinear flexural behaviour of corroded reinforced concrete beams*. *ACI Structural Journal* 102(4): 550-559
11. Huang, R. and Yang, C.C. 1997. *Condition Assessment of RC Beams Relative to Reinforcement Corrosion*. *Cement and Concrete Composites* 19: 131-137.
12. Imam, A., Anifowose, F. and Azad, A.K. 2015. *Residual strength of corroded reinforced concrete beams using an adaptive model based on ANN*. *International Journal of Concrete Structures and Materials* 9(2): 159-172.
13. Joyce, T. A. 2008. *The effect of steel reinforcement corrosion on the flexural capacity and stiffness of reinforced concrete beams*. Master thesis, Ryerson University, Toronto, Canada
14. Mangat, P.S., and Elgarf, M.S. 1999. *Flexural strength of concrete beams with corroding reinforcement*. In: *ACI Structural Journal* 96(1): 149-158
15. Rasheeduzzafar, Dakhil, F. H., and Al-Gahtani, A. S. 1985. *Corrosion of reinforcement in concrete structures in the middle east*. *Concrete International; American Concrete Institute* 7(9): 48-55.
16. Rodriguez, J., Ortega, L.M., and Casal, J. 1997. *Load carrying capacity of concrete structures with corroded reinforcement*. In: *Construction and Building Materials* 11(4): 239-248
17. Wang, X.H. and Liu, X.L. 2008. *Modeling the flexural carrying capacity of corroded RC beams*. *Journal of Shanghai Jiaotong University* 13(2): 129-135.
18. Wang, X. and Liu, X.L. 2010. *Simplified Methodology for the Evaluation of the Residual Strength of Corroded Reinforced Concrete Beams*. *Journal of Performance of Constructed Facilities* 24(2): 108-119.

THE EFFECT OF HYBRID STEEL FIBER ON CONCRETE PERFORMANCE

Ibim Green

Mechanical Engineering Technology, Federal Polytechnic of Oil and
Gas Bonny, Rivers State, Nigeria abba.green@yahoo.com

Kelechi Ugoji

Mechanical Engineering Technology, Federal Polytechnic of Oil and
Gas Bonny, Rivers State, Nigeria ugojic@yahoo.com

ABSTRACT

This study is aimed at examining the possible improvements on the fracture properties of concrete containing more than one fibre type. Several mixtures were elaborated in this study. To study the fracture properties and load resistance at various scales, discrete short brass fibres and double-hooked steel fibres were added in concrete. Different types of concrete mixtures were prepared and tested which contained varying proportions of steel and brass fibres up to 0.4% volume fraction. The effects of different hybrid fibre combinations at low and high dosages were investigated for compressive strength, splitting tensile strength and flexural strength. Test results indicated that the different hybrid fibre combinations played a significant crack arresting properties depending upon the fibre properties (size and fibre availability). The presence of steel fibres provided post crack resistance properties whereas the shorter brass fibres delayed the crack origination resulting in significant increase in mechanical strength. The hybrid fibre concretes containing steel fibres (0.3% Vf) and brass fibres (0.2% Vf) showed a consistent increase in the ultimate stress capacity up to 7.75% (in compression) and 37.98% (in fracture strength). Microscopic studies showed the effectiveness of different hybrid fibres during crack formation and subsequent propagation at different loading stresses. The use of steel fiber hybrid offers several economical and technical benefits.

Keywords: Compressive strength, Flexural strength, Steel fiber, Hybrid fiber, Concrete.

Introduction

The advancement in hybrid steel fibers improves the mechanical properties and the ductility of concrete structures. Fibre addition to concrete is a potential approach for enhancing the properties of hardened concrete. In recent years, there has been significant research conducted to study the effect of different fibres on the characteristics of hardened concrete. Steel fibres have traditionally been employed to improve crack resistance behaviour at various crack scales. The same factors that affect shrinkage strain in plain concrete also affect shrinkage strain in fibre reinforced concrete, including temperature and relative humidity, material properties, curing time, and structural size (Cunha et al 2009).

Studies have shown that adding fibres, particularly steel, to concrete has positive benefits in balancing the movements brought on by volume changes in concrete and tends to stabilize the volumetric changes sooner when compared to plain concrete. Steel fibres allow concrete to support several cracks, delay the

onset of the first crack, and greatly reduce crack widths (Ding et al 2010). Brittle tension failure with micro-level strains occurs in cement-based matrices. The tensile qualities of the FRC are significantly enhanced when discrete fibres are added to such matrices, whether continuous or discontinuous, as compared to the characteristics of the unreinforced matrix (Brouwers et al 2005). The characteristics have greatly improved because of a larger number of fibres present in the matrix along with a consistent load sharing system. To implicitly deduce the composite's tensile properties, the majority of FRC research relies on experimental observations from flexural or split cylinder tests (Petit et al 2010). The present study is conducted on the fracture resistance of brittle concrete composites using hybrid fibre combinations of steel and brass fibres. Fibres were also traditionally used in spatial distribution of concrete to achieve homogenous mechanical properties.

Objective of study

- (1) To conduct investigation on the fracture and ductile response of steel-brass hybrid fibre concretes at different volume fraction of fibres.
- (2) To systematically analyse the load carrying capacity of concretes containing different hybrid fibre combinations to evaluate its fracture efficiency and the optimal steel-brass fibre combination.
- (3) To analyse and interpret crack growth in various steel-brass hybrid fibre concrete system under monotonic flexural loading and fractured surfaces are interpreted with the advanced digital image analysis technique.

EXPERIMENTAL PROCEDURE

Materials

Concrete materials used consist of ordinary Portland cement, river sand as fine aggregates and crushed coarse aggregates from nearby source of granite rocks. Proportioning of concrete mixtures was done carefully in the ratio of 1:1.42:2.35 (Binder: Sand: Aggregate) at w/c ratio of 0.34. To achieve a high workable concrete mix up to 100 mm slump super-plasticizing admixtures were added. The various concrete mixtures are proportioned by varying the fibre content in terms of volume fraction of fibre dosage (% by volume of concrete). Short cut brass fibres of 6.54 mm long (average size) and double hooked steel fibres of 32 mm long were used in concrete mixes to evaluate the fibre synergy in the hardened concrete. The concrete manufacturing materials are provided in Table 1.

Table 1: Concrete manufacturing materials used.

Materials	Grade of material	Specific gravity	Particle size	Density (Kg/m ³)	Tensile Strength (N/mm ²)
Cement	43	3.12	0.0435	3215	-
Sand	3.12	2.45	2.61	2205	-
Crushed granite Aggregates	0.013	2.36	6.45	2415	-
Steel fibres	Double Hooked steel	7.34	L=32mm, D=0.35mm, Aspect ratio = 91	7450	440
Brass fibres	Loose stranded filaments	8.12	L=6.54mm, D=0.04mm, Aspect ratio = 164	8230	325

The various design concrete mix proportions for different hybrid fibre concrete mixes are as follows:

CASE 1: Plain Cement Concrete (PCC 1):

Cement - 342, Sand - 694, Coarse Aggregate - 1194, Water/Concrete ratio (w/c ratio) - 0.34, Water - 175, Superplasticizer – 24

CASE 2: Hybrid Steel Brass Fiber Concrete Two (HYSBFC-2):

Steel - 0.4% Vf, Brass - 0.1%Vf, Cement - 342, Sand - 694, Coarse Aggregate - 1194, Water/Concrete ratio (w/c ratio) - 0.34, Water - 175, Superplasticizer – 24

CASE 3: Hybrid Steel Brass Fiber Concrete Three (HYSBFC-3):

Steel - 0.3% Vf, Brass - 0.2%Vf, Cement - 342, Sand - 694, Coarse Aggregate - 1194, Water/Concrete ratio (w/c ratio) - 0.34, Water - 175, Superplasticizer - 24

CASE 4: Hybrid Steel Brass Fiber Concrete Four (HYSBFC-4):

Steel - 0.2% Vf, Brass - 0.3%Vf, Cement - 342, Sand - 694, Coarse Aggregate - 1194, Water/Concrete ratio (w/c ratio) - 0.34, Water - 175, Superplasticizer – 24

CASE 5: Hybrid Steel Brass Fiber Concrete Five (HYSBFC-5):

Steel - 0.1% Vf, Brass - 0.4%Vf, Cement - 342, Sand - 694, Coarse Aggregate - 1194, Water/Concrete ratio (w/c ratio) - 0.34, Water - 175, Superplasticizer - 24

Special chemical admixtures such as sulphonated melamine formaldehyde was added at 1% by weight of cement to reinstate the loss in consistency of fresh concrete. Fibres added in concrete mixes were known to show loss in consistency during fibre addition and this is effectively addressed by using superplasticizing admixtures. Freshly prepared concrete mixes were placed and compacted in the steel moulds as shown in Fig. 2 and allowed for normal drying in room temperature. After sufficient curing for a day, the moulds were removed to separate the hardened concrete and further kept under water curing for 28 days.



Fig. 2: Layered casting of concrete using steel-brass hybrids.

Laboratory testing of hybrid fibre composite beams

The specimens were tested in a universal compressive strength testing machine of 2000KN capacity which has an electronic digital controller for actuating the rate of loading, Also, the crack propagation in beams can be electronically tested using ultrasonic pulse velocity (UPV) measurements. The visual observations during first crack origination on the surface of concrete specimens were captured using digital recording machine for fracture assessment. Flexural testing of beam specimens of size 150×150×1000mm were carried out using a third point loading setup. Gradual loading rate of 0.5 mm/min was maintained throughout the bending test for maintaining a stable crack propagation and further crack bridging ability of brass fibres in the concrete matrix. To monitor the crack growth at the

centre it was intended to place the ultrasonic sensors using transducers at the middle third point of beam specimens. Digital images of concrete specimens were recorded to observe the crack propagation pattern in each type of concrete specimens. Fracture characteristics of concrete were assessed in terms of first crack origination and the fracture energy.

Digital images of sliced concrete specimens were taken at the fractured surfaces to assess the crack propagation patterns and fibre bridging mechanism. A digital USB Microscope of 1000x magnification with a resolution of 1280×960 pixels was used in this study to analyse the cracked surfaces in different concrete specimens. Microscopic images of failed concrete specimens were captured initially from cracked concrete sections and further image analysis were carried out.

RESULTS AND DISCUSSIONS

The influence of hybrid fibres in different failure loads of concrete are discussed in this section and the experimental values are represented in Fig. 3. It clearly indicated that compared to plain cement concrete, all fibre concretes showed controlled failure without any sudden cracking sound. A maximum compressive strength increases of 7.75% was noted in the case of steel-brass fibre concretes (HYSBFC-3). Also, the other hybrid fibre concretes reported a marginal increase in compressive strength without any abrupt strength loss. Fracture strength of all fibre incorporated concretes resulted in appreciable increase owing to additional reinforcing mechanism contributed by fibres. Maximum fracture strength of 7.12 N/mm² and 6.89 N/mm² was obtained for steel/brass hybrid concretes (HYSBFC-3 and HYSBFC-4 respectively) with an increase of 37.98% compared to plain concrete. It can be noted that hybrid fibre addition in concrete systems provided an appreciable increase in fracture strength. However, the presence of optimal fibre combination of 0.3% steel fibres and 0.2% brass fibres reported maximum strength up to 37.98%. Similar test observations were made by Cunha et al (2009) that high volume fraction of micro fibres may affect the post elastic strain hardening properties up to 60% in the strain capacity of composites. This was observed in the present study when the crack opening was unstable leading to increased crack width and hence the smaller micro brass fibres were not effective enough to bridge the widening cracks. Hence, it can be evident that the pre-peak strain hardening part is greatly influenced by short/micro brass fibres than longer steel fibres. This effectively provides matrix strengthening leading in delay in the origination of micro cracks. This also reveals that synergy of steel-brass hybrid fibre combinations are profoundly observed in all fibre combinations. The maximum ductility was observed for steel-brass hybrid fibre concrete (**HYSBFC-5**) up to 3.87mm with a maximum peak deflection of 2.13 mm. Since the post elastic deformation characteristics of fibre concretes were found to be dependent on the straining/yielding of fibres completely after failure. However, the straining of composite was found to be dependent on the number of fibres bridging the wider cracks as well as crack localization. In this study, it was apparently evident that maximum availability of brass fibres at crack opening provided adequate ductility leading to significant post elastic deformation.

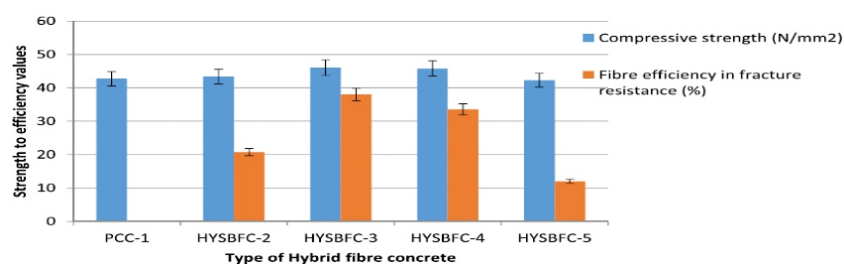


Fig. 3. Compressive strength to efficiency of hybrid fibre concretes.

However, the hybrid fibre efficiency in compression was found to be maximum of 7.75% and 7.23% for hybrid fibre concretes HYSBFC-3 and HYSBFC-4 respectively. Similar strength improvement upto 10% in flexural bending and fracture properties were reported in earlier studies [2,5,8,9] depending upon the type of hybrid fibre combinations used. Mechanism of hybrid fibres provide evidence that dual action of short and long fibres in arresting crack propagation at different scales and at different stress levels. Fibre effectiveness is also visibly observed depending upon the number of micro cracks appearing at maximum bending stress. This was visibly higher for steel-brass hybrids containing 0.1% steel fibres and 0.4% brass fibres as seen in Fig. 4. It can be inferred that by increasing fine brass fibres volume in the matrix comparatively to steel fibres, may result in higher bending resistance due to effective fibre bridging by shorter fibres. Many research studies conducted earlier support the hybrid fibre mechanism in concrete in terms of the careful selection of fibre types (length, aspect ratio, elastic modulus) and its volume fraction [10]. The dual fibre action noticed in this study proceeds at every crack interception and the effectiveness in synergistic crack arresting mechanism depends upon optimum volume fraction of steel (0.3%) and brass (0.2%) fibres.

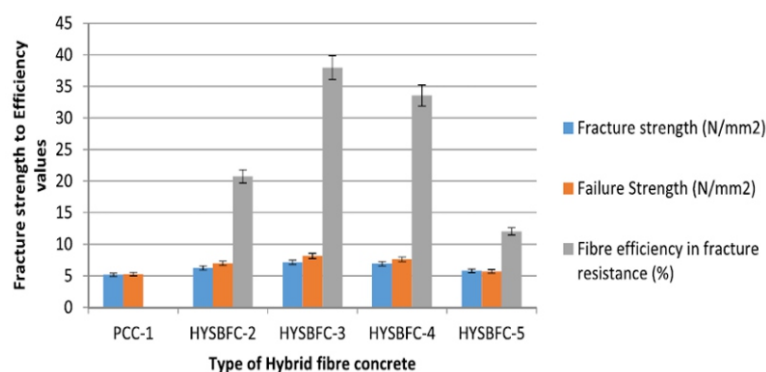


Fig. 4. Fracture strength to efficiency of hybrid fibre concretes.

The use of advanced image analysis at 500x magnification has provided distinctive fibre reinforcements in matrix phase and analysed for each type of hybrid fibre concrete specimen. The origination of steady state cracks occurs at the weak boundary of ITZ and propagates to the matrix phase. The various load levels were given to each concrete specimen to identify the potential cracking pattern as well as to observe the crack coalescing in the crack vicinity. It can be evidently seen that the crack coalescence occurs with either crack joining or leading to the origination of multiple cracking. At low stress levels up to 30% of ultimate load, the crack formation is slightly visible in the plain concrete specimens. The influence of fibres during crack origination is observed when the direction of propagation is controlled by the intercepting steel fibres. During stress transfer from the matrix to the fibres the interfacial shear stress is taken by fibres which may show debonding failure. The fibre effectiveness is pronounced when number of fibres provides crack bridging properties and has enhanced the load carrying capacity. In another research study, similar microscopic observations were made to analyse the fibre orientation and spacing on the fracture properties of concrete (Srinivasa et al 2009).

CONCLUSION

The experimental observations for different hybrid fibre concretes consisting of steel-brass fibre concretes were typically investigated in this study and summarized as given below.

- (1) Compressive strength of concrete is marginally improved depending upon the different hybrid substitutions and showed a maximum strength of 46.03 N/mm² (HYSBFC-3) with an increase upto 7.75%.

- (2) Hybrid Fibre efficiency in compressive performance was found to be marginal in the case of longer steel fibres which does not undergo required straining, whereas the presence of shorter/fine brass fibres in large availability provide adequate matrix strengthening leading to strength improvement.
- (3) The inclusion of hybrid fibres substantially increased the flexural performance and post crack performance of all hybrid fibre concretes without sudden cracking. Most notably a maximum failure strength up to 8.14 N/mm² was obtained for steel (0.3%) and brass (0.2%) hybrid concretes (HYSBFC-3).
- (4) A maximum efficiency of 37.98% and 33.53% in fracture resistance of hybrid fibre concretes was noticed in HYSBFC-3 and HYSBFC-4 concretes respectively. This showed effective synergistic combinations due to dual fibre mechanism played at different cracking scales. As the short and large availability of finer brass fibres provided high crack control mechanism at smaller micro-cracks and steel fibres provide adequate bridging mechanism upon increased crack widths.
- (5) The most important contribution of hybrid fibres mechanism was observed in terms of maximum ductility (3.87 mm) which was noticed in the case of steel-brass hybrids (HYSBFC-5) which exhibited a good post elastic deformation characteristics of hybrid fibre composites.
- (6) Microscopic image analysis showed convincing evidence of the dual role played by hybrid fibres during crack formation at low and high stress levels with a multi scale crack arresting properties in cementitious system.

REFERENCES

1. Ambroise J, Rols S and Pera J (2001). *Properties of self-leveling concrete reinforced by steel fibers. In Proceedings of 43rd Brazilian Congress of the Concrete (IBRACON), Brazil.*
2. Barr B, Gettu R, Al-Oraimi S K A, Bryars L S (1996). *Toughness measurement—the need to think again. Cement and Concrete Composites*, 18(4), 281-97.
3. Brouwers H.J.H and Radix H.J (2005). *Self-compacting concrete: theoretical and experimental study. Cement and Concrete Research*, 35(11), 2116-36.
4. Corinaldesi V and Moriconi G (2004). *Durable fiber reinforced self-compacting concrete. Cement and Concrete Research*, 34(2), 249-54.
5. Cunha V.M, Barros J.A and Sena-Cruz J.M (2009). *Pullout behaviour of steel fibers in self-compacting concrete. Journal of Materials in Civil Engineering*, 22(1), 1-9.
6. Dhonde H.B, Mo Y.L, Hsu T.T and Vogel J (2007). *Fresh and hardened properties of self-consolidating fiber reinforced concrete. ACI materials journal*, 104(5), 491–500.
7. Ding Y, You Z and Jalali S (2010). *Hybrid fiber influence on strength and toughness of RC beams. Composite Structures*, 92(9), 2083-9. 76 Haddadou et al., *J. Build. Mater. Struct.* (2014) 1: 65-76
8. Ding Y, You Z and Jalali S (2011). *The composite effect of steel fibres and stirrups on the shear behaviour of beams using self-consolidating concrete. Engineering Structures*, 33(1), 107.
9. Domeski J (2011). *Cracking moment in steel fiber reinforced concrete beams based on waste sand, OVIDIUS. University annals - constantza, series civil engineering*, XIII (13):29-34.
10. EFNARC (2005). *European guidelines for self-compacting concrete: Specification, production and use. Selfcompacting concrete, European Project Group.*
11. Elkhadiri I, Diouri A, Boukhari A, Aride J and Puertas F (2002). *Mechanical behaviour of various mortars made by combined fly ash and limestone in Moroccan Portland cement. Cement and Concrete Research*, 32(10), 1597-603.
12. Greenough T and Nehdi M (2008). *Shear behavior of fiber-reinforced self-consolidating concrete slender beams. ACI materials Journal*, 105(5), 468–77

13. Katzer J (2008). *Properties of precast SFRC beams under harmonic load*. *Science and Engineering of Composite Materials*, 15(2), 107-20.
14. Khayat K.H and Guizani Z (1997). *Use of viscosity-modifying admixture to enhance stability of fluid concrete*. *ACI Materials Journal*, 94(4), 332-41.
15. Moriconi G and Corinaldesi V (2005). *Rheological study of blended cement concrete*. In *proceeding: cement combinations for durable concrete*, edited by Dhir R.K. Harrison T.A., Newlands MD. The 6th Int. Congress on 'Global Construction: Ultimate Concrete Opportunities'. Thomas Telford, London, UK; p. 211-8.
16. Nagataki S and Fujiwara H (1995). *Self-compacting property of highly flowable concrete*. *ACI Special Publication*, 154, 301-14.
17. Okamura H and Ouchi M (2003). *Self-compacting concrete*. *Journal of Advanced Concrete Technology*, 1(1), 5-15.
18. Petit J.Y and Wirquin E (2010). *Effect of limestone filler content and superplasticizer dosage on rheological parameters of highly flowable mortar under light pressure conditions*. *Cement and Concrete Research*, 40(2), 235-41.
19. Şahmaran M, Christianto H.A and Yaman I.O (2006). *The effect of chemical admixtures and mineral additives on the properties of self-compacting mortars*. *Cement and concrete composites*, 28(5), 432-40.
20. Sahmaran M and Yaman I.O (2007). *Hybrid fiber reinforced self-compacting concrete with a high volume coarse fly ash*. *Construction and Building Materials*, 21(1), 150-6.
21. Srinivasa R, Sekhar T and Sravana P (2009). *Durability studies on glass fibre SCC*. *The Indian Concrete Journal*, 83(10), 44-52.
22. Torrijos M.C, Barragan B.E and Zerbino R.L (2008). *Physical-mechanical properties, and mesostructure of plain and fibre reinforced self-compacting concrete*. *Construction and Building Materials*, 22(8), 17808.

DEVELOPMENT OF ROBOTIC SYSTEM FOR SEGREGATION OF METALLIC COMPONENTS

Adyuth Hisham Babu Syed

Department of Robotics and Automation, PSG College of Technology,
Peelamedu, Coimbatore, 641004, Tamil Nadu, India *adyuthisham@gmail.com

Jonah N.

Department of Robotics and Automation, PSG College of Technology,
Peelamedu, Coimbatore, 641004, Tamil Nadu, India *nmn.rae@psgtech.ac.in

Binil Mohan

Department of Robotics and Automation, PSG College of Technology,
Peelamedu, Coimbatore, 641004, Tamil Nadu, India *bbiinniill100@gmail.com

ABSTRACT

The task of segregation of components is simple yet time-consuming. Automating such a task frees up time and resources to invest in other sectors. Pick and place operations performed by a robot reduce the workforce required and assure a degree of precision. In this paper, the different factors that come into play in designing a portable robotic system for pick and place operations were considered. The design focus was performing pick-and-place operations of components with ferromagnetic properties using object classification with a compact and portable nature. The developed robotic system included a microcontroller for controlling the robotic arm and a Raspberry Pi 4 for performing object classification. The portable system was built for performing the segregation of objects in a mobile manner. The robotic arm and other components were designed and selected for efficient performance.

Keywords: Robotic Arm, Raspberry Pi, Pico, TFLite

Introduction

As technology has progressed, robots have started performing significant roles in various sectors of different industries. Soon robots will be an irreplaceable part of society. One of the common use of robots is to perform pick and place operations. Robotic 2 arms are primarily engineered for industrial applications; however, there exists a growing demand for their utilization in residential and commercial settings as well. [1]. The main factors that are to be focused on when designing such a robot are the compactness, mobile nature of the device, the safety of the people around the device, the easy use of the robot, and aesthetics. Robotic systems are designed to meet specific requirements, primarily aimed at assisting and automating various tasks. The HSV colour detection algorithm was employed to effectively segregate coloured balls [2]. For object manipulation, the grain boundary function was employed to accurately determine the centroid of the ball, thus enabling the precise location estimation for pick and place operations. Waste segregation processes can be effectively automated through the implementation of robotic arms. Sensors were employed to identify the nature of waste materials for effective segregation [3]. Specifically, a moisture sensor and a metal sensor were utilized to discern wet

and metallic wastes, respectively. In an alternative method of waste segregation, convolutional neural network (CNN)-based classifiers were employed to determine the biodegradability of waste items [4]. The development of a robotic arm system dedicated to the segregation of common objects plays a significant role in minimizing the need for human labour in trivial tasks. The segregation task may seem trivial but it usually requires a person to perform it. Thus, by incorporating a robot to assist with the task, an additional workforce is freed up for other requirements. This paper presents the development of a robotic system specifically designed for the segregation of ferromagnetic components. The system employs a TFLite model for object identification, while a solenoid is utilized for object picking and segregation. The object identification model is deployed on a Raspberry Pi, while the design of the robotic arm prioritizes portability as a key consideration.

Implementation

As the objective of keeping the robotic system portable with minimal calibration, the components of the system must be compact and have minimal setup while having the resources for performing fast and precise actions. The selection of components required for the system was based on their optimal characteristics and suitability for the intended purpose.

Raspberry Pi 4

The Raspberry Pi 4 can run resource-intensive applications and multitask effectively. It is powered by a quad-core ARM Cortex-A72 processor with 8 GB RAM. For performing object classification, significant processing power is required for efficient and accurate classification. For modification of the classification set, the Pi 4 is accessible and easy to work with.

Raspberry Pi Pico

Selecting the appropriate microcontroller is a critical aspect as it is the core of the system. The main requirements of the microcontrollers are to efficiently perform the required tasks without taking up too much physical space. By selecting the best micro controller, the development process is streamlined, resulting in a more effective and fruitful system. Raspberry Pi Pico is a compact and inexpensive microcontroller. Pico has 264 kB of RAM and 2 MB of flash memory and is powered by a dual-core Arm Cortex-M0+ processor that operates up to 133 MHz [5]. The compact nature of the Pico and its high performance are the main highlights.



Figure 1: Robotic arm design.

Robotic Arm

Selecting the right robotic arm is of paramount importance in pick-and-place operations. The choice of

the robotic arm is determined by the arm's workspace and design. The robotic arm should ensure high repeatability and reliability. For the specific requirements of the robotic system, a robotic arm is 3D printed as shown in Figure 1 using the Anycubic Mega Pro. The robotic arm is modified such that the end effector has a slot for attaching the solenoid so that it acts as an electromagnet end effector.

Ultrasonic Sensor

The ultrasonic sensor utilizes sound waves to measure distances and detect objects in its vicinity. It emits high-frequency sound pulses and calculates the time it takes for the sound waves to bounce back after hitting an object. This data enables the sensor to determine the distance between itself and the object. The sensor sends a signal for the Pico to determine if an object is close enough for picking application.

Pi Camera Module

The camera module is an add-on designed for Raspberry Pi single-board computers. This compact camera module enables users to capture images and record videos directly from their Raspberry Pi. The camera module is compact in nature and the object classification is performed from the images captured from the camera module.

TensorFlow Lite

TFLite is a lightweight machine-learning framework designed specifically for edge models and mobile platforms. TFLite allows real-time inference and efficient memory utilization. The compact nature of the machine learning framework makes it easier to train and deploy on an edge device such as the Raspberry Pi 4.

Solenoid Electromagnet

The KK-P20 solenoid electromagnet shown in Figure 2 attracts magnetic substances using the induced magnetism produced by electric current. The solenoid can lift up to 3 Kg, thereby making it optimal for everyday objects like scissors and screws.



figure 2: KK-P20 solenoid.

Working Principle

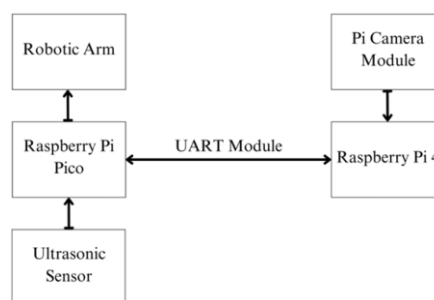


Figure 3: Block diagram.

The working principle of the robotic system developed for the segregation of components is presented in Figure 3. The main objective of the robotic system is to perform object segregation based on object type. To perform the tasks within the set parameters and while keeping the object portable the model is built in a compact design. The robotic arm is designed to be small yet able to carry the required loads. Object classification is performed on a Raspberry Pi 4 and Raspberry Pi Pico is used as the microcontroller for controlling the robotic arm. The functionality of the model is designed such that when an object is detected by the ultrasonic sensor, the Pico sends a signal to the Raspberry Pi to activate the camera module which captures an image of the object to be segregated. Data transfer between the Pico and Pi is performed using a UART module as shown in Figure 3. Both modules are set to receive and transmit data based on the requirements. A Tflite model is deployed in the Pi for the classification of the object. The identification of an object is performed by training the system using the data collected through the Pi Camera module. The object ID number is passed back to the Pico. Based on the object ID number, the Pico sends a command to the robotic arm to pick the object and segregate the object in a specified location which is calculated based on the number of objects to be segregated. The microcontroller is designed such that the robotic arm picks the object when the object ID is received. The solenoid is magnetized and the object is picked up and placed at the required location.

Microcontroller

The Raspberry Pi Pico acts as the central control unit for the robotic arm system. This microcontroller assumes responsibility for governing various modules within the system, including the robotic arm, ultrasonic sensor data acquisition, and activation of the electromagnet end effector as shown in Figure 4. Synchronization and control of all these distinct modules are achieved through the utilization of a micropython script. To ascertain the proximity of an object to the robotic arm, a predefined threshold is established for the ultrasonic sensor. Upon receiving distance data from the ultrasonic sensor, if the measured distance falls below this threshold, the presence of an object is detected. Subsequently, a UART protocol is employed to transmit a signal to the Raspberry Pi 4, triggering the magnetization of the Solenoid through the utilization of a relay.



Figure 4: Robotic arm prototype.

Robotic Arm

The robotic arm comprises three servos and is equipped with an electromagnet end effector (Figure 5). The robotic arm is programmed for performing pick and place operations and performing object

segregation based on the type of object detected. On startup, the robotic arm moves to its home position. When an object is detected by the ultrasonic sensor a signal is sent to the Pi 4 for object classification. The drop locations for each object are calculated on startup based on the number of objects to be segregated. The object is picked up by the electromagnet and dropped at the designated location based on the identified object class. After successfully dropping, the robotic arm is moved back to its home position and is set on standby till another object is detected.

Object Classification

Machine learning is crucial in the efficient detection and separation of different components. For the present system, there are a few criteria to be met. Timely and precise identification and separation of components are the main necessity. The trained model must be deployed on edge devices. In the present system, a TFLite model is deployed for object classification. TFLite is a collection of tools to convert and optimize TensorFlow models to run on mobile and edge devices [6]. A custom model is trained based on the required object to be segregated. The object classification model is deployed on the Raspberry Pi 4 and the Pi Camera module is used for acquiring images. When an object is detected by the ultrasonic sensor, the Pico sends a signal to the Pi 4 to perform object classification. The camera module is activated and the object is identified as shown in Figure 6. After successful classification, the object ID is passed back to the Pico through the UART protocol for object segregation.



Figure 5: Object classification.

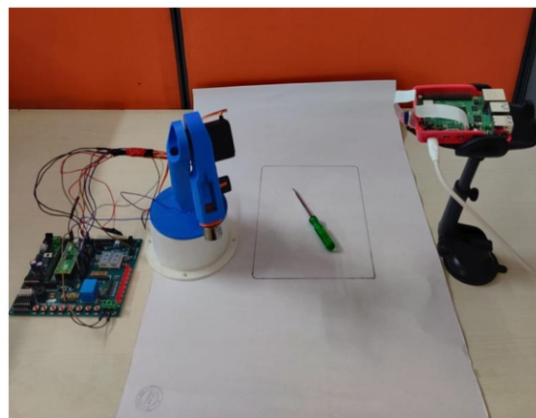


Figure 6: Project setup.

Results

The developed robotic system is displayed in Figure 7. The system has been tested for three objects; screwdriver, scissor, and battery (Figure 8). The Raspberry Pi 4 is externally powered and the Raspberry Pi Pico is powered by the Pi. On startup, the robotic arm is moved to a home position. When the ultrasonic sensor detects an object, a signal is sent to the Raspberry Pi 4 for performing object classification. The classification ID is sent to the Pico and the robotic arm picks and places the object in a precalculated position.

Conclusion

A robotic system for the segregation of the components was developed using a robotic arm, a microcontroller, an ultrasonic sensor, and a camera. It was trained to identify three components and the system was tested to segregate the components. It was found that the robotic system performed well for the purpose for which it was developed.

References

- [1] Wongphati, M., Matsuda, Y., Osawa, H., & Imai, M. (2012, September). *Where do you want to use a robotic arm? And what do you want from the robot? 2012 IEEE RO-MAN: The 21st IEEE International Symposium on Robot and Human Interactive Communication*. PP 324 9
- [2] Chhabra, M., Gupta, A., Mangal, A., & Reel, P. S. (2011). *Segregation of colored objects using industrial robotic arm. Communications in Computer and Information Science*, 759–761.
- [3] E. K. D. More, S. Divya, G. Kalyani, and R. Gowthami, *Automatic Waste Segregator Bin Using Robotic Arm*. 2018.
- [4] S. Nandhini, S. Mrinal, N. Balachandran, K. Suryanarayana, and D. S. H. Ram, *Electronically assisted automatic waste segregation*. 2019.
- [5] *Raspberry Pi Documentation - Raspberry Pi Pico and Pico W*. (n.d.). *Raspberry Pi Documentation - Raspberry Pi Pico and Pico W*.
- [6] *TensorFlow Lite*. (n.d.). *TensorFlow*.

Instructions for Authors

Essentials for Publishing in this Journal

- 1 Submitted articles should not have been previously published or be currently under consideration for publication elsewhere.
- 2 Conference papers may only be submitted if the paper has been completely re-written (taken to mean more than 50%) and the author has cleared any necessary permission with the copyright owner if it has been previously copyrighted.
- 3 All our articles are refereed through a double-blind process.
- 4 All authors must declare they have read and agreed to the content of the submitted article and must sign a declaration correspond to the originality of the article.

Submission Process

All articles for this journal must be submitted using our online submissions system. <http://enrichedpub.com/> . Please use the Submit Your Article link in the Author Service area.

Manuscript Guidelines

The instructions to authors about the article preparation for publication in the Manuscripts are submitted online, through the e-Ur (Electronic editing) system, developed by **Enriched Publications Pvt. Ltd.** The article should contain the abstract with keywords, introduction, body, conclusion, references and the summary in English language (without heading and subheading enumeration). The article length should not exceed 16 pages of A4 paper format.

Title

The title should be informative. It is in both Journal's and author's best interest to use terms suitable. For indexing and word search. If there are no such terms in the title, the author is strongly advised to add a subtitle. The title should be given in English as well. The titles precede the abstract and the summary in an appropriate language.

Letterhead Title

The letterhead title is given at a top of each page for easier identification of article copies in an Electronic form in particular. It contains the author's surname and first name initial .article title, journal title and collation (year, volume, and issue, first and last page). The journal and article titles can be given in a shortened form.

Author's Name

Full name(s) of author(s) should be used. It is advisable to give the middle initial. Names are given in their original form.

Contact Details

The postal address or the e-mail address of the author (usually of the first one if there are more Authors) is given in the footnote at the bottom of the first page.

Type of Articles

Classification of articles is a duty of the editorial staff and is of special importance. Referees and the members of the editorial staff, or section editors, can propose a category, but the editor-in-chief has the sole responsibility for their classification. Journal articles are classified as follows:

Scientific articles:

1. Original scientific paper (giving the previously unpublished results of the author's own research based on management methods).
2. Survey paper (giving an original, detailed and critical view of a research problem or an area to which the author has made a contribution visible through his self-citation);
3. Short or preliminary communication (original management paper of full format but of a smaller extent or of a preliminary character);
4. Scientific critique or forum (discussion on a particular scientific topic, based exclusively on management argumentation) and commentaries. Exceptionally, in particular areas, a scientific paper in the Journal can be in a form of a monograph or a critical edition of scientific data (historical, archival, lexicographic, bibliographic, data survey, etc.) which were unknown or hardly accessible for scientific research.

Professional articles:

1. Professional paper (contribution offering experience useful for improvement of professional practice but not necessarily based on scientific methods);
2. Informative contribution (editorial, commentary, etc.);
3. Review (of a book, software, case study, scientific event, etc.)

Language

The article should be in English. The grammar and style of the article should be of good quality. The systematized text should be without abbreviations (except standard ones). All measurements must be in SI units. The sequence of formulae is denoted in Arabic numerals in parentheses on the right-hand side.

Abstract and Summary

An abstract is a concise informative presentation of the article content for fast and accurate Evaluation of its relevance. It is both in the Editorial Office's and the author's best interest for an abstract to contain terms often used for indexing and article search. The abstract describes the purpose of the study and the methods, outlines the findings and state the conclusions. A 100- to 250-Word abstract should be placed between the title and the keywords with the body text to follow. Besides an abstract are advised to have a summary in English, at the end of the article, after the Reference list. The summary should be structured and long up to 1/10 of the article length (it is more extensive than the abstract).

Keywords

Keywords are terms or phrases showing adequately the article content for indexing and search purposes. They should be allocated heaving in mind widely accepted international sources (index, dictionary or thesaurus), such as the Web of Science keyword list for science in general. The higher their usage frequency is the better. Up to 10 keywords immediately follow the abstract and the summary, in respective languages.

Acknowledgements

The name and the number of the project or programmed within which the article was realized is given in a separate note at the bottom of the first page together with the name of the institution which financially supported the project or programmed.

Tables and Illustrations

All the captions should be in the original language as well as in English, together with the texts in illustrations if possible. Tables are typed in the same style as the text and are denoted by numerals at the top. Photographs and drawings, placed appropriately in the text, should be clear, precise and suitable for reproduction. Drawings should be created in Word or Corel.

Citation in the Text

Citation in the text must be uniform. When citing references in the text, use the reference number set in square brackets from the Reference list at the end of the article.

Footnotes

Footnotes are given at the bottom of the page with the text they refer to. They can contain less relevant details, additional explanations or used sources (e.g. scientific material, manuals). They cannot replace the cited literature.

The article should be accompanied with a cover letter with the information about the author(s): surname, middle initial, first name, and citizen personal number, rank, title, e-mail address, and affiliation address, home address including municipality, phone number in the office and at home (or a mobile phone number). The cover letter should state the type of the article and tell which illustrations are original and which are not.

[illegible]